

Turbulent Marginal Separation and the Turbulent Goldstein Problem ^{*}

Bernhard Scheichl[†] and Alfred Kluwick[‡]

Vienna University of Technology, A-1040 Vienna, Austria

A new rational theory of incompressible turbulent boundary layer flows having a large velocity defect is presented on basis of the Reynolds-averaged Navier–Stokes equations in the limit of infinite Reynolds number. This wake-type formulation allows for, among others, the prediction of singular solutions of the boundary layer equations under the action of a suitably controlled adverse pressure gradient which are associated with the onset of marginally separated flows. Increasing the pressure gradient locally then transforms the marginal-separation singularity into a weak Goldstein-type singularity occurring in the slip velocity at the base of the outer wake layer. Interestingly, this behavior is seen to be closely related to (but differing in detail from) the counterpart of laminar marginal separation where the skin friction replaces the surface slip velocity. Most important, adopting the concept of locally interacting boundary layers results in a closure-free and uniformly valid asymptotic description of boundary layers which exhibit small closed reverse-flow regimes. Numerical solutions of the underlying triple-deck problem are discussed.

Nomenclature

\hat{A}	Displacement function (TD theory), Eqs. (99), (117)
\hat{B}	Slope of \hat{U}_s near separation (TD theory), Eq. (129)
\hat{B}_1	Leading-order coefficient in expansion of \hat{B} about $\hat{L} = \chi - \chi^* = 0$, Eqs. (129), (131)–(133)
\hat{L}	Bubble length, Eq. (128)
\hat{P}	Induced pressure, Eq. (101)
\hat{s}, \hat{x}	Shifted streamwise coordinates, Eq. (41)
\hat{X}, \hat{Y}	LD coordinates (TD theory), Eqs. (94), (113), (114)
\hat{y}	Vertical UD coordinate, Eq. (106)
\hat{Z}	Shifted LD coordinate (TD theory), Eq. (127)
\mathcal{X}, \mathcal{Y}	Transformed LD coordinates, Eq. (120)
\tilde{L}, \tilde{U}	Reference length, reference velocity
A	Displacement function (BL theory), Eq. (50)
$A_{+, -}$	Numerical constants, Eqs. (26), (87)
B	Upstream slope of U_s , Eq. (28)
b	Constant slope $d\Delta/dx$ (self-preserving BL solution)
C_+	Numerical constant, Eq. (92)
c_ℓ	Constant in mixing length closure by Michel et al.
D	Strength of perturbation of B , Eq. (33)
F	Stream function (self-preserving BL solution)
f, \bar{f}	Stream functions (locally expanded BL solutions), Eqs. (18), (20), (21), (56)
$F_{+, -}$	Leading-order stream functions (locally expanded BL solutions), Eqs. (23), (25)

^{*}This work has been presented in the *Memorial Session for Dr. Dave Walker* of the 4th AIAA Theoretical Fluid Mechanics Conference, 6–9 June 2005, Toronto, Ontario, Canada, and is a revised, refined, and slightly extended version of the AIAA paper 2005-4936.

[†]Postdoctoral Research Fellow, Vienna University of Technology, Institute of Fluid Mechanics and Heat Transfer, Resselgasse 3/E322, A-1040 Vienna, Austria, e-mail: b.scheichl@tuwien.ac.at.

[‡]Full Professor, Vienna University of Technology, Institute of Fluid Mechanics and Heat Transfer, Resselgasse 3/E322, A-1040 Vienna, Austria, e-mail: a.kluwick@tuwien.ac.at, Senior AIAA member.

G	Stream function perturbation (locally expanded BL solutions), Eq. (80)
g, \check{g}	Stream function perturbations (locally expanded BL solutions), Eqs. (31), (35), (36)
H	Auxiliary function
h	Surface metric coefficient
I	Intermittency factor, Eq. (12)
k	Surface curvature
l	Local sublayer thickness, Eq. (18)
m	External flow exponent, Eq. (13)
m_s	External flow exponent (self-preserving BL), Eq. (13)
p	Pressure
r	Exponent, Eq. (56)
Re	Reynolds number (globally defined), Eq. (1)
s	Local streamwise coordinates, Eq. (15)
S, \hat{S}	Local streamwise LD coordinates, Eqs. (55), (129)
T	Reynolds shear stress (BL solution), Eq. (6)
t, z	Auxiliary variables
u', v'	Velocity fluctuations in x - and y -direction
U, P	Local representations of $u_e, dp/dx$, Eq. (14)
u, v	Velocity components in x - and y -direction
U_+	Numerical constant, Eq. (26)
u_e	Surface slip velocity (external potential flow), Eq. (7)
U_s	Surface slip velocity (BL solution), Eq. (10)
u_s	Surface slip velocity, Eq. (88)
X, \bar{Y}	LD coordinates (BL theory), Eq. (43)
x, y	Natural coordinates
Y	BL coordinate, Eq. (5)

Subscripts

$+, -$	Downstream and upstream (of $s = 0$ or $\hat{s} = 0$) evolving forms
D, R	Detachment, reattachment
G, M	Goldstein-type singularity, marginal-separation singularity
i	i th member in asymptotic series
ij	j th member of i th member in asymptotic series
ijk	k th member of j th member of i th member in asymptotic series

Conventions

$\bar{\Psi}, \bar{T}$	LD representations (BL theory) of Ψ and T , Eq. (44)
\bar{U}_s	LD representation (BL theory) of U_s , Eq. (48)
$\hat{\psi}, \hat{p}$	UD perturbations of ψ , Eq. (107), and p , Eq. (108)
$\hat{\Psi}, \hat{T}$	LD representations (TD theory) of Ψ , Eqs. (113), (114), and T , Eq. (115)
\hat{U}_s	LD representation (TD theory) of U_s , Eq. (122)
\star	Dependences on unknown quantities
q	Notation to represent a collection of quantities
$\langle q \rangle$	Reynolds-averaging of any quantity represented by q
$1a, 1b$	Oncoming near-surface flow regimes (BL theory)
2	Downstream and upstream evolving main flow regimes (BL theory)
I	Lower deck
II	Main deck
III	Upper deck
BL	Boundary layer
IW	Inner wake
LD	Lower deck
OW	Outer wake
TD	Triple-deck
TST	Transcendentally small terms
UD	Upper deck

Symbols

α	Slenderness parameter
β	Control parameter, Eq. (13)
χ	Coupling parameter, Eq. (93)
χ_b	Upper bound of χ , Eq. (95)
δ	BL thickness
ℓ	Mixing length, Eq. (8)
ϵ	Bifurcation parameter (redefined), Eq. (42)
ε	Notion for gauge function, Eqs. (18), (31)
$\eta, \hat{\eta}$	Similarity variables based on s , Eq. (19), and \hat{s} , Eq. (77)
$\bar{\eta}, \check{\eta}, \tilde{\eta}$	Similarity variables, Eqs. (30), (35), (55)
Γ	Gamma function
γ	Bifurcation parameter, Eq. (15)
κ	V. Kármán constant, Eqs. (11), (135)
λ, μ	Invariance parameters, Eq. (120)
ω	Exponent, Eqs. (31), (36)
ϕ	Local scaling function, Eqs. (35), (37)
ψ	Stream function
ρ, ϑ	Polar coordinates, Eq. (71)
$\hat{\rho}, \vartheta$	Polar coordinates (UD), Eq. (110)
σ	TD length scale, Eq. (94)
τ	Surface friction, Eq. (135)
θ	Heaviside function
$\tilde{\nu}$	Kinematic viscosity
Δ	BL thickness (BL solution), Eq. (6)
Γ	Upstream limit of \hat{U}_s , Eqs. (94), (118), (124)
Λ	Strength of induced pressure, Eqs. (96), (101), (115)
Ω	Eigenvalue
Ψ	Stream function (BL solution), Eq. (6)
Υ	Shear stress gradient evaluated at surface, Eq. (126)
Ξ, Φ	Coefficients in asymptotic series, Eq. (127)
ξ	BL coordinate related to Δ , Eq. (12)
ζ	Auxiliary variable

Superscripts

*	Onset of separation
---	---------------------

I. Introduction

A Tribute to the Work of Professor Dr. David Walker on Turbulent Boundary Layers

THE method of matched asymptotic expansions has undoubtedly proven very successful not only in gaining a profound understanding of laminar high-Reynolds-number flows in many aspects but also in providing a rational framework for a methodical and comprehensive treatment of turbulent shear layers. It is to Prof. David Walker's credit that he was one of the first to have elucidated the modern and fruitful asymptotic formulation of the classical two-dimensional two-tiered turbulent boundary layer structure which is essentially based on the assumption of an asymptotically small streamwise velocity defect with respect to the external free-stream flow, see the extensive contribution Ref. 1. For an extension to the three-dimensional case the reader is referred to Ref. 2 and Ref. 3, and a summary is also given in Ref. 1. In contrast to earlier treatments of wall-bounded turbulent shear flows put forward in the pioneering papers by, among others, Yajnik,⁴ Bush and Fendell,⁵ Fendell,⁶ and Mellor,⁷ in his thorough analysis the local (and not a characteristic) value of the skin friction velocity serves as the principal perturbation parameter. That is, leading- and higher-order contributions to the well-established logarithmic law of the wall are effectively summed up to a single leading-order expression whereas higher-order corrections are free of purely logarithmic terms. In turn, the logarithmic law of the wall appears as the limit far from the surface of the leading-order streamwise velocity distribution inside the viscous wall layer. Hence, the whole information needed for the further analysis of the

outer velocity defect layer is subsumed in a single term in an elegant manner. We note that this formulation was also adopted by Gersten^{8,9} and, more recently, in the further developments by the present authors.^{10–12} Also, a more recent strong experimental support of that classical scaling is found in Ref. 13.

Moreover, it must be emphasized that David Walker was substantially involved in providing the initial steps towards a systematic insight into the very complex turbulent near-wall dynamics by investigating the unsteady Navier–Stokes equations in the high-Reynolds-number limit.^{1,14–17}

Despite the undeniable progress, where much of it must be attributed to David Walker, asymptotic methods have contributed towards an understanding of the fundamental physics of wall-bounded turbulent shear flows, a fully self-consistent theory describing turbulent boundary layer separation in the limit of high Reynolds number is not available at the moment. In particular, the literature lacks a rational description of the, from an engineering point of view, very important case of separation from a smooth surface which is caused by a smooth adverse pressure gradient, imposed by the external flow. In laminar boundary layer theory this type of separation is commonly referred to as *marginal* separation as the boundary layer may exhibit a closed reverse-flow regime at its base if the pressure gradient is properly chosen. This theory was developed independently by Ruban^{18,19} and by Stewartson et al.,²⁰ also cf. Ref. 21. However, a systematic approach to its turbulent counterpart has been hampered severely by the fact that, generally spoken, turbulent boundary layers are known to be less prone to separate than the corresponding laminar ones, owing to the enhanced wall shear stress. More specifically, the classical small-defect formulation is seen to withstand a smooth adverse pressure gradient as the wall shear stress remains constant in the high-Reynolds-number limit. Furthermore, the velocity defect solution in the outer main layer is characterized by linearized convective terms in leading order, which indicates that it does not terminate in a singularity during downstream evolution. As a matter of fact, this property is demonstrated numerically in the preliminary work provided by Ref. 10,22 for the present investigation. Additionally, the study of turbulent separation past a blunt body by Neish and Smith²³ serves as a further strong hint that the classical description of a turbulent boundary layer exposed to a smooth adverse pressure gradient predicts firmly attached flows which do not separate at all (apart from the inevitable flow detachment close to the rear stagnation point as it is the case in the situation considered in Ref. 23) in the limit of high Reynolds number.

The first systematic approach, however, to tackle the challenging problem of pressure-induced turbulent separation from an asymptotic viewpoint was carried out by Melnik.^{24,25} He proposed a primary expansion of the flow quantities in terms of a small parameter, denoted by α , which measures the slenderness of the boundary layer and is contained in all commonly employed shear stress closures and/or fixed by experiments. For example, in case of the algebraic mixing length model by Michel et al.^{8,26} it is identified with the square of the constant $c_\ell \approx 0.085$. Most important, its value appears to be essentially independent of the Reynolds number as the latter may take on arbitrarily large values. Specifically, Melnik adopted Clauser's²⁷ early idea of adopting the laminar-like well-known algebraic eddy-viscosity closure for the Reynolds shear stress. We note that Clauser already concluded on semi-empirical grounds in his seminal investigation²⁷ that, in definite contrast to the laminar case, for turbulent boundary layer flows the thereby defined Reynolds number given by $1/\alpha$ remarkably takes on a fixed value. By assuming a (non-dimensional) velocity defect of $O(1)$ in the main body of the boundary layer, that strategy is seen to provide a powerful tool for constructing a rational novel description of turbulent boundary layers, which predicts wake-type wall-bounded flows in the limit of infinite Reynolds number and even allows for the treatment of marginal separation.

Among others, a cornerstone of Melnik's analysis is the prediction of a square-root singularity encountered by the slip velocity at the base of the outermost wake region of the boundary layer as separation is approached due to the occurrence of an Eulerian flow stage close to the surface. This result may be regarded as the turbulent counterpart to the celebrated Goldstein singularity^{28,29} in laminar boundary layer theory where the slip velocity is replaced by the wall shear stress. Rather remarkable, however, it has recently been shown^{12,22} that the pressure gradient can be controlled in a way such that the Goldstein-type singularity eventually disappears: then the slip velocity decreases regularly, vanishes in a single point but increases rapidly immediately further downstream, giving rise to an abrupt acceleration of the flow near the surface. In turn, this situation is associated with *turbulent marginal* separation.

Unfortunately, Melnik's theory^{24,25} is not only incomplete as it does not give a hint how to surmount that separation singularity within the framework of the Reynolds-averaged Navier-Stokes equations but remains conceptually unsatisfactory, also for a number of additional reasons:

- (i) In definite contrast to the primary premise of α being independent of the globally defined Reynolds number Re as $Re \rightarrow \infty$, the approach implies that $\alpha^{1/2} \ln Re = O(1)$ in order to account for the well-

known logarithmic near-wall portion of the streamwise velocity holding upstream of separation.

- (ii) The formation of a square-root singularity in the slip velocity which also includes the effects due to the Reynolds shear stress gradient must be taken into account, in principle. Therefore, if the Eulerian limit holds indeed (independent of a specific closure), the theory lacks an explanation why such a more general form of a singularity does not occur.
- (iii) It remains unclear how far the asymptotic flow structure and the main results depend on Melnik's choice of the algebraic eddy-viscosity-based closure for the Reynolds shear stress in the outer wake regime.

The novel theory to be presented here is based on Melnik's formulation of turbulent boundary layers having a large velocity defect, strikingly contrasting the classical asymptotic theory. Most important, however, it also copes with the issues (i)–(iii). In the subsequent analysis we concentrate on the case $\alpha \ll 1$ at infinite Reynolds number, formally written as $Re^{-1} = 0$.

The paper is organized as follows: In §II the essential basic assumptions underlying the theory and their implications are presented. In §III we give a short survey of the numerical study of a boundary layer driven by a controlled pressure gradient towards marginal separation and the local analysis of the flow near the point of vanishing slip velocity. A particular form is assumed for the external flow velocity in terms of a single parameter, such that the local adverse pressure gradient increases as this parameter increases. For a critical value of the parameter, a singularity appears at a certain location, indicating the first appearance of separation. As the parameter is increased slightly, the singularity is shifted a short distance upstream. The singular behavior of the flow near this point of vanishing slip velocity is summarized. Such an investigation has already been presented in Ref. 22 and will also be outlined, more extensively, in a separate investigation. The key results of the work are provided by §IV, where we focus on the local interaction of the marginally separating boundary layer with the induced external irrotational flow. The local flow is seen to have a three-layer, or *triple-deck*, structure; the appropriate limiting forms of the basic equations are presented for the different flow regions. As a highlight, akin to the laminar case,^{19,20} a fundamental equation governing turbulent marginal separation, which is independent of a specific shear stress closure, is derived, and its solutions are discussed. Representative numerical results are shown, demonstrating the extent of the asymptotically short and flat separation bubble.

II. Motivation and Problem Formulation

A. Governing Equations

We consider a nominally steady and two-dimensional fully developed turbulent boundary layer driven by an incompressible and otherwise non-turbulent external bulk flow along a smooth and impermeable solid surface, being e.g. part of a diffuser duct, see figure 1: Let x , y , u , v , u' , v' , and p denote plane natural coordinates, respectively, along and perpendicular to the surface given by $y = 0$, the time-mean velocity components in x - and y -direction, the corresponding turbulent velocity fluctuations, and the time-mean fluid pressure. These quantities are non-dimensional with a reference length \tilde{L} characteristic for the mean velocity variation of the bulk flow along the surface (and the surface geometry), a reference value \tilde{U} of the surface slip velocity due to the prescribed inviscid and irrotational external free stream flow, and the uniform fluid density. The (constant) kinematic fluid viscosity $\tilde{\nu}$ and \tilde{L} , \tilde{U} then define a suitable global Reynolds number Re , which is taken to be large,

$$Re = \tilde{U} \tilde{L} / \tilde{\nu} \rightarrow \infty. \quad (1)$$

We furthermore introduce a stream function ψ by

$$\partial\psi/\partial y = u, \quad \partial\psi/\partial x = -h v, \quad h = 1 + k(x) y. \quad (2)$$

Here $k(x) = O(1)$ is the non-dimensional surface curvature, where the cases $k < 0$, $k = 0$, and $k > 0$ refer to a concave, plane, and convex surface, respectively, cf. figure 1. Adopting the usual notation for the turbulent

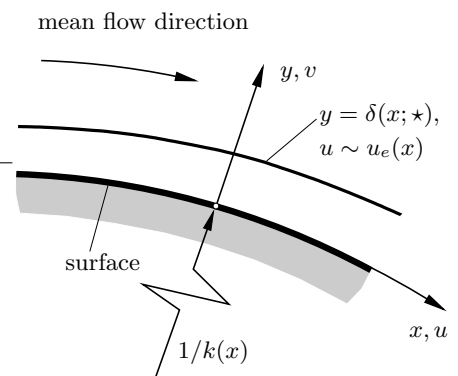


Figure 1. Flow configuration, here shown for $k(x) > 0$.

stresses, the dimensionless time- or, equivalently, Reynolds-averaged Navier–Stokes equations then read (cf. Ref. 8, p. 81)

$$h \left(\frac{\partial \psi}{\partial y} \frac{\partial}{\partial x} - \frac{\partial \psi}{\partial x} \frac{\partial}{\partial y} \right) \frac{\partial \psi}{\partial y} - k \frac{\partial \psi}{\partial x} \frac{\partial \psi}{\partial y} = -h \frac{\partial p}{\partial x} - h \frac{\partial \langle u'^2 \rangle}{\partial x} - \frac{\partial h^2 \langle u'v' \rangle}{\partial y} + O(Re^{-1}), \quad (3)$$

$$\left(\frac{\partial \psi}{\partial x} \frac{\partial}{\partial y} - \frac{\partial \psi}{\partial y} \frac{\partial}{\partial x} \right) \left(\frac{1}{h} \frac{\partial \psi}{\partial x} \right) - k \left(\frac{\partial \psi}{\partial y} \right)^2 = -h \frac{\partial p}{\partial y} - \frac{\partial h \langle v'^2 \rangle}{\partial y} - \frac{\partial \langle u'v' \rangle}{\partial x} + k \langle u'^2 \rangle + O(Re^{-1}). \quad (4)$$

Herein the terms of $O(Re^{-1})$ refer to the divergence of the viscous stresses, which are presumed to be negligibly small compared to the Reynolds stresses throughout the boundary layer with the exception of a viscous sublayer adjacent to the surface.

B. A Novel Wake-like Limit of Wall-Bounded Turbulent Shear Flows

A new approach to turbulent boundary layers has been developed in order to provide an appropriate asymptotic concept for a description of marginally separated flows. This theory is essentially founded on three key assumptions (which, although seeming plausible, nevertheless have to be validated empirically):

- (i) Both the velocity fluctuations u' and v' are of the same order of magnitude in the limit $Re \rightarrow \infty$, so that all Reynolds stress components are scaled equally in the whole flow field. This requirement for local isotropy in the limit (1) is invoked quite frequently in the further analysis but will not be addressed again then.
- (ii) As the basic property of the flow and already mentioned in the introduction, the streamwise velocity deficit in the main part of the boundary layer, where Reynolds shear predominates over molecular shear, is a quantity of $O(1)$.
- (iii) The distance $y = \delta(x; \star)$, here the asterisk shall indicate any further dependences, from the surface defines the time-mean outer edge of the boundary layer, as sketched in figure 1 on the preceding page. This is in agreement with the observation of a rather sharp fluctuating outer edge of the time-dependent fluid motion.

1. Leading-Order Boundary Layer Problem

As a first consequence of the items (i)–(iii), inspection of the equations of motion (3) and (4) suggests a shear layer approximation, where the slenderness of the associated boundary layer is measured by a small positive parameter, denoted by $\alpha \ll 1$, such that $\delta = O(\alpha)$. We, therefore, anticipate inner expansions

$$y = \alpha Y, \quad (5)$$

$$\{\psi, -\langle u'v' \rangle, \delta\} = \alpha \{\Psi(x, Y), T(x, Y), \Delta(x)\} + O(\alpha^2), \quad (6)$$

$$p - p_0(x) = O(\alpha) \quad \text{where} \quad dp_0/dx = -u_e du_e/dx = O(1). \quad (7)$$

Herein $u_e(x)$ denotes the surface velocity imposed by the external potential bulk flow. Then, the main flow regime of the boundary layer is governed by the boundary layer equation

$$\frac{\partial \Psi}{\partial Y} \frac{\partial^2 \Psi}{\partial Y \partial x} - \frac{\partial \Psi}{\partial x} \frac{\partial^2 \Psi}{\partial Y^2} = u_e \frac{du_e}{dx} + \frac{\partial T}{\partial Y}, \quad T = \ell^2 \frac{\partial^2 \Psi}{\partial Y^2} \left| \frac{\partial^2 \Psi}{\partial Y^2} \right|, \quad (8)$$

where the latter relationship defines the mixing length ℓ . Equation (8) is subject to the wake-type boundary conditions

$$\Psi(x, 0) = T(x, 0) = 0, \quad \frac{\partial \Psi}{\partial Y}(x, \Delta(x)) - u_e(x) = T(x, \Delta(x)) = 0. \quad (9)$$

The requirements to be satisfied at the boundary layer edge given by $y = \delta(x; \alpha, \star)$, cf. figure 1 on the previous page, or, equivalently, $Y \sim \Delta(x)$, reflect the patch with the irrotational external flow, and the conditions holding at the base of the outer wake arise from the match with the α - and Re -dependent sublayers. These are not considered here in detail but are discussed in, respectively, Ref. 11 and Ref. 12 (and, in a more comprehensive manner, in a separate study) and outlined briefly in § II.B.2.

Note that the solution in the outer wake region comprising most of the boundary layer is completely determined by Eqs. (8) and (9). As an important consequence arising from the boundary conditions (9), a solution of Eq. (8) gives rise to an in general non-vanishing slip velocity

$$U_s = \frac{\partial \Psi}{\partial Y}(X, 0), \quad (10)$$

in agreement with the boundary layer concept already proposed by Clauser.²⁷ We expect non-trivial solutions of Eqs. (8) and (9), i.e. wake-type solutions having $U_s \neq u_e$ and $T \neq 0$. In other words, inside the boundary layer the simple irrotational Eulerian, i.e. non-turbulent, time-mean limit of the Navier–Stokes equations, which implies $\partial u / \partial Y \equiv 0$ and, consequently, $u = \partial \Psi / \partial Y \equiv u_e(x)$, is disregarded.

2. Does the Boundary Layer Thickness Depend on Re ?

Highly remarkably, dimensional reasoning and order-of-magnitude analysis suggests that the last of the boundary conditions (9) is fully equivalent to a negation of this question as far as the limit $Re \rightarrow \infty$ is concerned. As expressed by the last statement in the foregoing paragraph, the assumed streamwise velocity deficit of $O(1)$ implicates that the Reynolds equations (3) and (4) admit a further limit apart from the pure Eulerian one, such that the slenderness parameter α remains indeed finite even in the formal limit $Re^{-1} = 0$.

The rationale can be subsumed as follows:^{8,10–12} Dimensional and scaling arguments strongly indicate that the mixing length satisfies the well-known v. Kármán’s near-wall law. Using the present notation, it is written as

$$\ell \sim \kappa Y / \alpha^{1/2}, \quad Y / \alpha^{1/2} \rightarrow 0, \quad (11)$$

where κ denotes the v. Kármán constant. The relationship (11) holds in the overlap conjoining the fully turbulent part of the boundary layer and the viscous sublayer, where the molecular shear stress has the same magnitude as its turbulent counterpart.^{8,10–12} The celebrated logarithmic law of the wall is fully equivalent to the behavior of the mixing length given by Eq. (11). However, since it clearly prevents matching the flow quantities in the main part of the boundary layer and the viscous sublayer, at least one additional intermediate layer has to be introduced which provides the linear decay of the mixing length predicted by Eq. (11) at its base. Regarding the main layer, the assumed velocity defect of $O(1)$ together with the resulting homogeneous boundary conditions holding for $Y \rightarrow 0$, see Eq. (9), then strongly suggest the absence of a viscosity-affected turbulent velocity scale in the outer main layer (as will be outlined in greater detail in a separate publication dealing with finite-Reynolds-number effects, see also Ref. 11,12). That is, the stream function there and, as the most important consequence, the boundary layer thickness δ are unaffected by the surface friction and thus by the strongly Reynolds-number-affected flow close to the surface, at the least to leading order. Therefore, the scaling parameter α is seen to be independent of Re as $Re \rightarrow \infty$, and the shear stress tends to zero as $Y \rightarrow 0$.

Furthermore, we note that the mixing length ℓ is supposed to admit a finite limit in the overlap with an inner wake layer where the scaled wall distance $Y / \alpha^{1/2}$ is of $O(1)$. In turn, ℓ is a quantity of $O(1)$ in both the main and the intermediate layer. There the convective terms are linearized since $u \sim U_s(x)$, as the turbulent velocity scale, which also measures the velocity perturbations about the slip velocity U_s , appears to be of $O(\alpha^{3/4})$. We emphasize that the here proposed behavior of ℓ is corroborated by any commonly applied mixing length closure, see the rather simple algebraic model by Michel et al.,^{8,26} for instance. Then the in Eq. (8) included balance between convection and the Reynolds shear stress gradient requires that the width of the latter region is of $O(\alpha^{3/2})$. As α does not depend on Re , the Reynolds shear stress in that layer still does not match the asymptotically constant shear stress in the viscous near-wall region. Consequently, this indicates that both flow regimes are not influenced by viscous effects in leading order and are, therefore, identified as an outer and inner wake layer, respectively, see figure 2. It is interesting to note that the resulting asymptotic structure of the boundary layer then closely

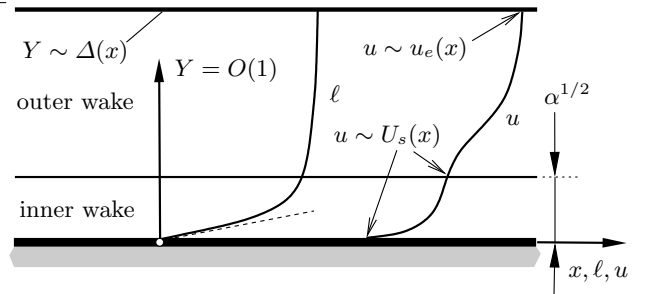


Figure 2. Two-tiered asymptotic splitting of the boundary layer and schematic distribution of the streamwise velocity u and the mixing length ℓ in the formal limit $Re^{-1} = 0$. The dashed asymptote refers to Eq. (11).

resembles that of a turbulent free shear flow, which was investigated by Schneider.³⁰ One major difference is the surface effect expressed by Eq. (11), giving rise to a square-root behavior of $u^{8,10,11}$ at the base of the inner wake regime, as sketched in figure 2 on the previous page, which has originally been established to hold on top of the viscous sublayer in case of a separating boundary layer, see e.g. Ref. 8. Hence, for finite values of Re a further layer emerges between the viscous sublayer and the inner wake region. Therein the Reynolds shear stress matches the wall shear stress but varies linearly with distance from the surface.^{10–12} In view of the subsequent analysis, however, it is sufficient to consider the outer wake layer only. As mentioned before, here the analysis of the remaining flow regimes is relegated to Ref. 11,12 (as well as a more detailed separate publication).

III. Singular Solutions of the Boundary Layer Equations

Since it provides the motivation of the present analysis, it is useful to present a brief survey of Ref. 22. In this connection we stress that we are interested primarily in particular solutions of Eqs. (8) and (9) where $U_s(x)$ vanishes locally, indicating the onset of separation.

A. Weakly Singular Numerical Solutions

In order to complete the turbulent boundary layer problem, Eqs. (8) and (9) are supplemented with the simple mixing length model

$$\ell = I(\xi) \Delta(x), \quad I(\xi) = 1/(1 + 5.5 \xi^6), \quad \xi = Y/\Delta(x), \quad (12)$$

where the well-known intermittency factor $I(\xi)$ by Klebanoff³¹ accounts for the decrease of the mixing length (and thus for an improved flow prediction) near the boundary layer edge, cf. the experimental data presented in Ref. 32. In fact, calculations employing the classical almost constant mixing length distribution in the outermost region,⁸ recovered for $I \equiv 1$, yield a slightly slower decay of the streamwise velocity near $y = \Delta(x)$ and appear to overestimate the boundary layer thickness function $\Delta(x)$. Note that the in the model (12) predicted proportionality of ℓ and the boundary layer thickness is the asymptotic representation for the outer wake layer of any well-known algebraic mixing length closure. As an example, for the case $I \equiv 1$ the relationship (12) is easily obtained from the model by Michel et al.^{8,26} by formally taking the limit $c_\ell \rightarrow 0$. As already stated in the introduction, here α is taken to be c_ℓ^2 .

Numerical solutions of the problem posed by Eqs. (8), (9), and (12) were obtained for retarded external flows which are assumed to be controlled by two parameters m_s and β , which e.g. characterize the diffuser shape, by specifying distributions of u_e of the form

$$u_e(x; m_s, \beta) = (1 + x)^{m(x; m_s, \beta)}, \quad \frac{m}{m_s} = 1 + \frac{\beta}{1 - \beta} \theta(2 - x) [1 - (1 - x)^2]^3, \quad m_s < 0, \quad 0 \leq \beta < 1. \quad (13)$$

Here $\theta(t)$ denotes the Heaviside function where $\theta = 0$ for $t < 0$ and $\theta = 1$ for $t \geq 0$. It is expected, however, that other choices neither of $u_e(x)$ nor of the mixing length closure (12) will affect the behavior of the solution near the location where $U_s = 0$ significantly. We also note with respect to the imposed velocity distribution (13) that in the case $\beta = 0$, i.e. $m \equiv m_s$, the boundary layer equations (8) and (9) admit self-similar solutions $\Psi = \Delta F(\xi)$, $\Delta = b(1 + x)$, where $b = \text{const}$ and the position $x = -1$ defines the virtual origin of the flow, if $m_s > -1/3$. Then both the linear growth b of the boundary layer thickness and the exponent m_s are functions of $F'(0)$, leading to a slip velocity $U_s \propto (1 + x)^m F'(0)$.^{8–10,22} These solutions were used to provide initial conditions at $x = 0$ for the downstream integration of Eqs. (8), (9), and (12) with u_e given by Eq. (13). The calculations were started by prescribing a rather small velocity defect characterized by $F'(0) = 0.95$ at $x = 0$, which in turn yields $b \doteq 0.3656$ and $m_s \doteq -0.3292$. Computations were then carried out for a number of positive values of the control parameter β . Inspection of Eq. (13) shows that the exponent m then varies within the range $0 < x < 2$ and thus causes an additional deceleration of u_e there. The key results which are representative for the responding boundary layer are displayed in figure 3 on the following page (a).

If β is sufficiently small, the distribution of U_s is smooth, and $U_s > 0$ throughout. However, if β reaches a critical value $\beta_M \doteq 0.84258$, the surface slip velocity U_s is found to vanish at a single location $x = x_M$ but is positive elsewhere. A further increase of β provokes a breakdown of the calculations, accompanied with the formation of a weak singularity slightly upstream at $x = x_G$. An analogous behavior is observed for the boundary layer thickness Δ , which is smooth in the sub-critical case $\beta < \beta_M$, exhibits a rather sharp peak for

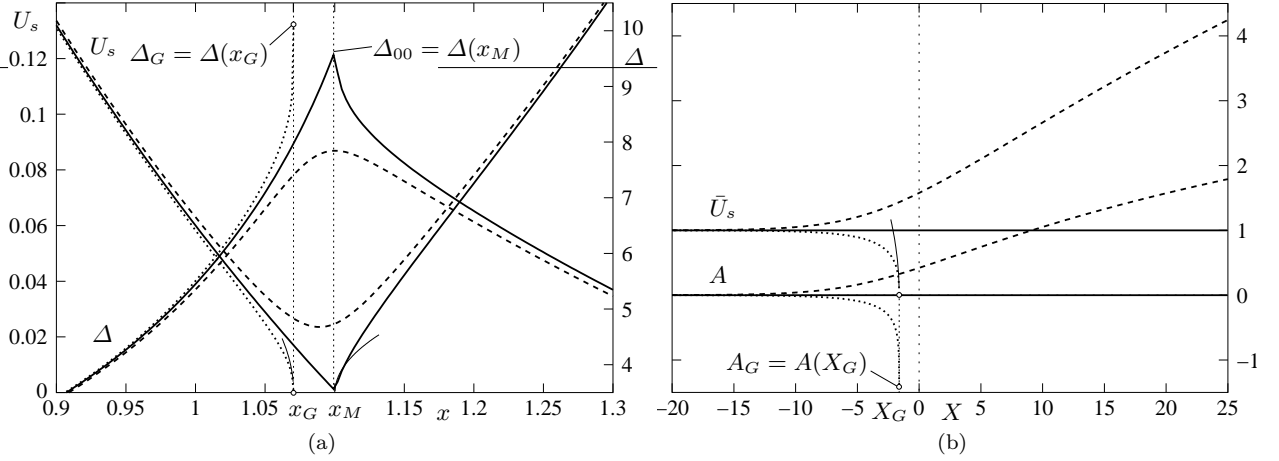


Figure 3. Critical (solid), sub- (dashed), and super-critical (dotted) boundary layer solutions: (a) $\beta \approx \beta_M \doteq 0.84258$ (solid), $\beta = 0.8422$ (dashed), $\beta = 0.8428$ (dotted), (b) canonical representation.

$\beta = \beta_M$ at $x = x_M$, and approaches a finite limit Δ_G in an apparently singular manner in the super-critical case $\beta > \beta_M$.

Following the qualitatively similar behavior of the wall shear stress which replaces the slip velocity in the case of laminar boundary layers,¹⁸ here the critical solution is termed a *marginally* separating boundary layer solution. However, in vivid contrast to its laminar counterpart,¹⁸ it is clearly seen to be locally asymmetric with respect to the critical location $x = x_M$ where it is singular. Moreover, the turbulent solutions appear to be highly sensitive numerically to very small deviations from $\beta = \beta_M$ as $x - x_M \rightarrow 0_-$. As will turn out in the following, these closely related properties reflect the basic mechanism governing the flow in the limits $x \rightarrow x_M$ and $\beta \rightarrow \beta_M$, which is vastly different from the laminar case.

B. The Marginal-Separation Singularity

To study the local flow behavior near $x = x_M$ both the outer-edge velocity u_e and the pressure gradient dp_0/dx given by Eq. (7) are Taylor-expanded as

$$u_e = U_{00} + sU_{01} + \gamma U_{10} + \cdots, \quad dp_0/dx = P_{00} + \gamma P_{10} + \cdots, \quad P_{00} = -U_{00}U_{01}, \quad P_{10} = -U_{10}U_{01}, \quad (14)$$

where the perturbation parameters s and γ are defined by

$$s = x - x_M \rightarrow 0, \quad \gamma = \beta - \beta_M \rightarrow 0. \quad (15)$$

At first we focus on the critical case $\gamma = 0$. Then both the quantities Ψ and Δ are seen to assume a finite limit,

$$\Psi(x, Y) \rightarrow \Psi_{00}(Y), \quad \Delta(x) \rightarrow \Delta_{00} \quad \text{as } s \rightarrow 0, \quad (16)$$

see figure 3 (a) and figure 4 on page 11, and, in agreement with the considerations pointed out in § II.B.2, inspection of Eq. (12) indicates the important relationships

$$\ell(x, Y) \rightarrow \ell_0(Y) \quad \text{as } s \rightarrow 0, \quad \ell_0 \rightarrow \ell_{00} = O(1) \quad \text{as } Y \rightarrow 0. \quad (17)$$

Equation (17) provides the only empirical parameter ℓ_{00} entering the local analysis. Note that in particular the latter relationship in Eq. (17) is not only merely a consequence of the specific closure adopted, cf. Eq. (12). It rather is a consequence of the behavior of the mixing length, which, related to the two-tiered splitting of the wake regime of the boundary layer as sketched in figure 2, characterizes the outer wake layer.

We furthermore mention that, as a result of the limits assumed in (16) and (17), in both the main regions 2_- and 2_+ where $Y = O(1)$, see figure 4 on page 11, their perturbations for small values of s are governed by the convective operator in Eq. (8) only. Due to the singular behavior of the boundary layer

solution as $s \rightarrow 0$ one has to expect the occurrence of disturbances in the expansion of Ψ about its finite limit $\Psi_{00}(Y)$ which vanish as $s \rightarrow 0$ and are proportional to $\Psi'_{00}(Y)$. These perturbations represent local eigensolutions of the linear operator obtained from the corresponding linearization of Eq. (8) where $\ell = \ell_0(Y)$. However, as they do not satisfy the boundary conditions at $Y = 0$, expressed by Eq. (9), they singularly perturb that limiting value Ψ_{00} , such that for sufficiently small values of Y at least one sublayer has to be considered. There the Reynolds stress term comes into play in leading order as it contains the highest derivative of Ψ with respect to Y . But that means that there exists a region of a local thickness, say, $l(s)$ where in leading order a balance between the nonlinear convective terms and the Reynolds shear stress gradient, as provided by Eq. (8), is maintained. Then the stream function there is locally expanded as

$$\Psi = l(s)\varepsilon(s)f_0(\eta) + \dots, \quad d \ln \varepsilon / ds \sim l^{-3} \quad \text{as } \varepsilon, l \rightarrow 0, \quad s \rightarrow 0. \quad (18)$$

The boundary conditions (8) require $f_0(0) = f'_0(0) = 0$. A careful investigation (to be presented in a separate study) of the resulting boundary value problem determining $f_0(\eta)$ in the case $s \rightarrow 0_-$ shows that, in order to provide a match with the expansion of Ψ about $\Psi_{00}(Y)$ in the main region 2_- , also the pressure gradient has to enter the aforementioned leading-order balance expressed by the second relationship in Eq. (18). The gauge function ε for the streamwise velocity component then is taken proportional to $(-s)^{1/2}$, giving $l \propto (-s)^{1/3}$. As a result, the momentum balance (8) is fully retained in the regions $1a_-$ and 1_+ , see figure 4, where the wall coordinate

$$\eta = Y / (\ell_{00}^{2/3} |s|^{1/3}) \quad (19)$$

is a quantity of $O(1)$. In these flow regimes then the following expansions hold in, respectively, the upstream and the downstream case,

$$s \rightarrow 0_- : \quad \frac{\Psi}{\ell_{00}^{2/3} P_{00}^{1/2}} = (-s)^{5/6} f_{0-}(\eta) + (-s)^{4/3} f_{1-}(\eta) + \dots, \quad (20)$$

$$s \rightarrow 0_+ : \quad \frac{\Psi}{\ell_{00}^{2/3} P_{00}^{1/2}} = s^{5/6} f_{0+}(\eta) + \dots, \quad (21)$$

and the resulting boundary value problem for $f_{0\mp}(\eta)$ reads

$$\begin{aligned} 1/2 f''_{0\mp} - 5/6 f_{0\mp} f''_{0\mp} &= \pm 1 \mp (f''_{0\mp})', \\ \eta = 0 : f_{0\mp} = f''_{0\mp} = 0, \quad \eta \rightarrow \infty : f_{0\mp} &= O(\eta^{5/2}), \end{aligned} \quad (22)$$

where the upper and lower signs refer to the cases $s \rightarrow 0_-$ and $s \rightarrow 0_+$, respectively. The conditions at $\eta = 0$ follow from the wake-type boundary conditions (9), and the requirement for $\eta \rightarrow \infty$ reflects the match with the flow regimes 2_- and 2_+ , see figure 4 on the next page, where the relations (16) and (17) hold. It can be shown (as will be demonstrated in a separate paper) that in the upstream case the problem (22) has only the obvious solution

$$f_{0-} = F_-(\eta) = 4/15 \eta^{5/2}, \quad (23)$$

which expresses a balance between the Reynolds shear stress gradient and the adverse pressure gradient at the surface for vanishing convective terms. In turn, the match with the marginally separating profile $\Psi_{00}(Y)$ of the stream function implies

$$\Psi_{00} \sim \frac{4}{15} \frac{P_{00}^{1/2}}{\ell_{00}} Y^{5/2}, \quad Y \rightarrow 0, \quad (24)$$

and $f_{0+} \sim F_-(\eta)$ as $\eta \rightarrow \infty$. However, in the case $s \rightarrow 0_+$ a combined analytical and numerical investigation reveals a single (strictly positive) non-trivial solution, denoted by $F_+(\eta)$, that has to be calculated numerically,²²

$$f_{0+} = F_+(\eta), \quad \eta \rightarrow \infty : F_+ = 4/15 (\eta + A_+)^{5/2} + \text{TST}, \quad (25)$$

where TST means transcendentally small terms. It is found that

$$A_+ \doteq 1.0386, \quad U_+ = F'_+(0) \doteq 1.1835. \quad (26)$$

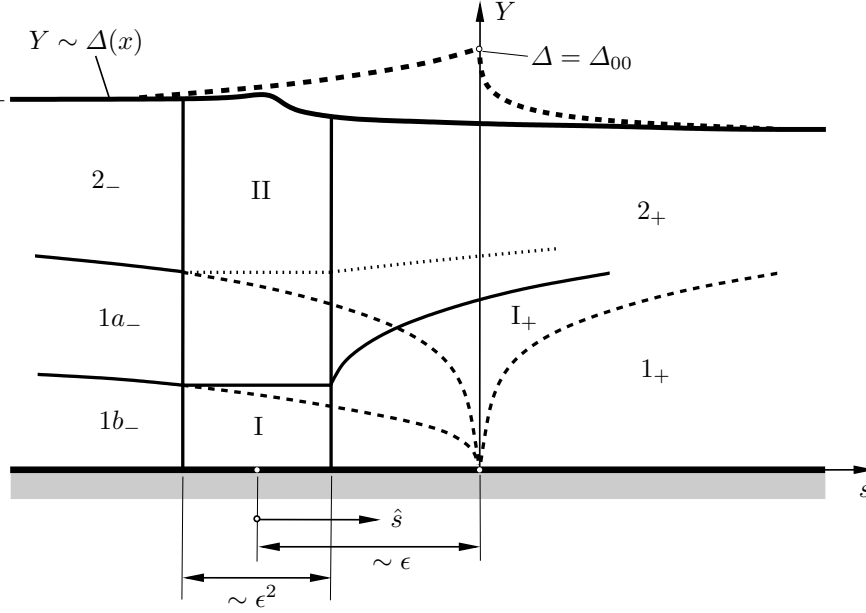


Figure 4. Asymptotic splitting of the oncoming (subscripts $-$) and downstream evolving (subscripts $+$) boundary layer flow in the formal limit $Re^{-1} = 0$, double-deck structure (lower deck I, main deck II). The case $\gamma \neq 0$ is sketched using solid lines, whereas the limiting structure for $\gamma = 0$ characterizing marginal separation is drawn using dashed lines partly. The flow regimes the extent of which is marked by dotted lines are seen to behave passively and are thus not considered in the text.

As a result of the leading-order analysis, turbulent marginal separation is seen to be associated with a purely regular behavior of the flow upstream of $s = 0$ as expressed by the higher-order term in the expansion (20). Substitution into Eq. (8) yields

$$f_{1-} = B \left(\eta + \frac{\eta^4}{180} \right), \quad B > 0, \quad (27)$$

where the constant B characterizing the slope $dU_s/ds \sim -BP_{00}^{1/2}$ of the linearly decreasing slip velocity in the limit $s \rightarrow 0_-$ must be determined numerically from the oncoming flow, cf. the upstream distribution of U_s in figure 3 (a). That is, the flow is locally governed by the eigensolutions $f_{0-}(\eta)$, $f_{1-}(\eta)$, and $f_{0+}(\eta)$, so that

$$s \rightarrow 0_- : U_s/P_{00}^{1/2} = -Bs + \dots, \quad (28)$$

$$s \rightarrow 0_+ : U_s/P_{00}^{1/2} = U_+ s^{1/2} + \dots, \quad (29)$$

Hence, the existence of the non-trivial downstream solution turns out to be responsible for the (infinitely) strong acceleration of the flow immediately downstream of the location $s = 0$ due to the irregular behavior of U_s , see Eq. (29). In turn, the convective part in Eq. (8) evaluated at $Y = 0$, given by $U_s dU_s/dx$, exhibits a jump at $s = 0$ from 0 to the value $P_{00}U_+^2/2$ in leading order. By adopting the numerical value $P_{00} \doteq 0.02272$, the downstream asymptote (29) is plotted as a thin solid line in figure 3 (a).

The fact that convection does not vanish necessarily at the surface $Y = 0$ not only causes the inherently nonlinear downstream behavior, governed by Eq. (22), in contrast to the theory of laminar marginal separation,^{18,19} but also gives rise to a fundamentally different analysis of the perturbed case $\gamma \neq 0$.

C. Bifurcating Flow for $\gamma \neq 0$

1. Exponentially Growing Eigensolutions

The contributions given by Eqs. (23) and (27) to the expansion (20) become of the same order of magnitude at distances s where the new variable

$$\bar{\eta} = \eta/(-B^2s)^{1/3} \quad (30)$$

is a quantity of $O(1)$. This situation forces a further sublayer $1b_-$, see figure 4 on the preceding page, where the gradients of the Reynolds shear stress and the pressure dominate over convection. Furthermore, the most rapidly downstream growing perturbations possible are assumed to originate in this layer as their s -derivatives may become asymptotically larger than the disturbances itself there, such that convection comes into play again very close to the surface. This thereby anticipated balancing of the perturbed convective and Reynolds stress terms is required by the boundary conditions holding for $\bar{\eta} \rightarrow 0$. These considerations and inspection of the boundary layer equations (8) and (9) then imply that the strongest perturbations are proportional to $\varepsilon(s)g(\bar{\eta})$, where the gauge function $\varepsilon(s)$ satisfies the estimate $s^2 d\varepsilon/ds = O(\varepsilon)$ and $g(\bar{\eta})$ denotes a shape function. Also, these perturbations must be due to the terms proportional to γ in Eq. (14). In turn, this suggests the following expansion in the region $1b_-$,

$$\begin{aligned} \Psi/[\ell_{00}^{2/3} P_{00}^{1/2} (-Bs)^{5/3}] &= F_-(\bar{\eta}) + \bar{\eta} + \dots + \varepsilon(s)g(\bar{\eta}) + \dots, \\ \varepsilon(s) &= -\gamma \exp \omega(s), \quad \omega(s) = \Omega/(-B^2s) + o(1/s), \quad \Omega > 0. \end{aligned} \quad (31)$$

The higher-order contributions to the exponent $\omega(s)$ then must be determined by analyzing the higher-order terms in the expansion (31) by means of the Fredholm alternative in order to investigate the consecutive inhomogeneous problems (this is a topic of current research, see also Ref. 22). The eigenvalue Ω , however, is fixed by the solution of the leading-order eigenvalue problem for the eigensolution $g(\bar{\eta})$, found by linearization of Eqs. (8) and (9),

$$\Omega [(2/3)\bar{\eta}^{3/2} + 1]g' - \bar{\eta}^{1/2}g = 2(\bar{\eta}^{1/2}g'')', \quad g(0) = g''(0) = 0, \quad g'(0) = D > 0. \quad (32)$$

Here the unknown constant D is assumed to be fixed by the oncoming flow, such that the expansion (28) is perturbed according to

$$U_s/P_{00}^{1/2} = -Bs[1 - \gamma D \exp \omega(s)] + \dots. \quad (33)$$

A numerical study shows that problem (32) allows for a solution $g(\bar{\eta})$ having sub-exponential growth for $\bar{\eta} \rightarrow \infty$ solely in the case $\Omega = 1/3$. Moreover, only in that case the solution of problem (32) has been found analytically. It reads

$$g(\bar{\eta})/D = \frac{2}{3} \bar{\eta} \exp(-\bar{z}) + \left(\frac{2}{9}\right)^{1/3} \left(\frac{2}{3} \bar{\eta}^{3/2} + 1\right) \int_0^{\bar{z}} t^{-1/3} \exp(-t) dt, \quad \bar{z} = \frac{2}{9} \bar{\eta}^{3/2}. \quad (34)$$

In turn, the associated perturbation in expansion (31) provokes also exponentially small disturbances in the flow regimes $1a_-$ and $1b_-$, respectively, and in the distribution of the boundary layer thickness $\Delta(x)$.

The question arises if there exist further perturbations if $\gamma \neq 0$ in the region $1b_-$ which locally grow faster than that considered above and are, therefore, responsible for a breakdown of the asymptotic flow structure holding in the limit $\gamma = 0$. Consequently, we complete the analysis of the class of eigensolutions that exhibit exponential growth as $s \rightarrow 0_-$ by scrutinizing the possibility of the generation of disturbances proportional to γ which originate in a region located even closer to the surface than is the flow regime $1b_-$, see figure 4 on the previous page. This is accomplished by the introduction of the new local variables

$$\check{\eta} = \bar{\eta}/\phi(-s), \quad \check{g}(\check{\eta}) = g(\bar{\eta}), \quad (35)$$

which are assumed to be quantities of $O(1)$. The latter relationship in Eq. (35) expresses the match of the (for the present analysis here unknown) shape function $g(\bar{\eta})$ of the respective perturbation in region $1b_-$ with that considered here, denoted by $\check{g}(\check{\eta})$. Independent of the specific choice of the (positive) function $\phi(-s)$, substitution of the coordinate stretching (35) into the boundary layer equations Eqs. (8) and (9) is seen to be consistent with the generalized form

$$\frac{\check{\Psi}}{\ell_{00}^{2/3} P_{00}^{1/2} (-Bs)^{5/3} \phi} = \check{\eta} + \phi^3 F_-(\check{\eta}) + \dots - \gamma \exp \omega(s) \check{g}(\check{\eta}) + \dots, \quad \frac{1}{\omega(s)} \rightarrow 0_+ \quad \text{as } s \rightarrow 0_-, \quad (36)$$

of the expansion (31). In the limit

$$\phi(-s) \rightarrow 0_+ \quad \text{as} \quad s \rightarrow 0_- \quad (37)$$

under consideration the balance between the perturbations of $O(\gamma)$ of the convective terms and the Reynolds stress gradient requires to write

$$\omega = \omega_0(s) + o(\omega_0), \quad s \rightarrow 0_-, \quad (38)$$

where ϕ can always be scaled such that

$$\omega'_0(s) = (Bs)^{-2} \phi(-s)^{-3}, \quad s \rightarrow 0_-. \quad (39)$$

Then the associated disturbances having a growth rate $\omega'(s)$ given by Eqs. (38) and (39) which is stronger than that implied by the expansion (31) are found to be governed by a reduced form of the problem (32). Integrated once, it reads

$$\check{g} = 2\check{\eta}^{1/2}\check{g}'', \quad \check{g}(0) = \check{g}''(0) = 0, \quad \check{g}'(0) > 0. \quad (40)$$

However, the solution of problem (40) exhibits exponential growth for $\check{\eta} \rightarrow \infty$. Consequently, no eigensolutions with a growth rate stronger than that given by Eq. (31) are generated.

2. Canonical Boundary Layer Solutions

The expansion (31) ceases to be valid within region I, the so-called lower deck, see figure 4 on page 11, where the gauge function ε has become a quantity of $O(1)$. As a consequence of its exponential growth, that region of non-uniformity takes place an asymptotically small extent upstream of $s = 0$ where $-B^2s \sim \Omega/\ln(1/\gamma)$. With respect to the further analysis, this behavior then is conveniently expressed by introducing the coordinate shift

$$\hat{s} = s + \varepsilon/B, \quad \hat{x} = x + \varepsilon/B, \quad (41)$$

see figure 4, and considering the limit

$$\varepsilon = \Omega/(B \ln |D/\gamma|) \rightarrow 0, \quad \Omega = 1/3. \quad (42)$$

Substitution of the variables

$$X = \frac{\hat{s}}{\varepsilon^2}, \quad \bar{Y} = \frac{Y}{(\ell_{00}\varepsilon)^{2/3}}, \quad \bar{\Psi}(X, \bar{Y}) = \frac{\Psi}{\ell_{00}^{2/3} P_{00}^{1/2} \varepsilon^{5/3}}, \quad (43)$$

which are quantities of $O(1)$ in the flow regime I, into Eqs. (8) and (9) yields to leading order the reduced, i.e. canonical, equations

$$\frac{\partial \bar{\Psi}}{\partial \bar{Y}} \frac{\partial^2 \bar{\Psi}}{\partial \bar{Y} \partial X} - \frac{\partial \bar{\Psi}}{\partial X} \frac{\partial^2 \bar{\Psi}}{\partial \bar{Y}^2} = -1 + \frac{\partial \bar{T}}{\partial \bar{Y}}, \quad \bar{T} = \frac{\partial^2 \bar{\Psi}}{\partial \bar{Y}^2} \bigg|_{\frac{\partial^2 \bar{\Psi}}{\partial \bar{Y}^2}}, \quad (44)$$

subject to the boundary conditions

$$\bar{Y} = 0 : \quad \bar{\Psi} = \bar{T} = 0, \quad (45)$$

$$\bar{Y} \rightarrow \infty : \quad \partial \bar{T} / \partial \bar{Y} - 1 \rightarrow 0, \quad (46)$$

$$X \rightarrow -\infty : \quad \bar{\Psi} \rightarrow F_-(\bar{Y}) + \bar{Y} - \text{sgn}(\gamma) \exp(X/3) g(\bar{Y}). \quad (47)$$

It is furthermore useful to define the rescaled slip velocity

$$\bar{U}_s = \frac{\partial \bar{\Psi}}{\partial \bar{Y}}(X, 0), \quad (48)$$

which serves to expand U_s ,

$$U_s = \varepsilon P_{00}^{1/2} \bar{U}_s(x) + \dots, \quad (49)$$

and the displacement function

$$A(X) = \lim_{\bar{Y} \rightarrow \infty} (\bar{T} - \bar{Y}). \quad (50)$$

By matching with the flow in the main deck II, see figure 4 on page 11, one obtains

$$\bar{\Psi} = \bar{\Psi}_{00}(Y) + \epsilon^{2/3} \ell_{00}^{2/3} A(X) \bar{\Psi}'_{00}(Y) + \dots + (\epsilon - \epsilon^2 B \hat{X}) \bar{\Psi}_{01}(Y) + \dots \quad (51)$$

In turn, applying the boundary conditions given by Eq. (9) which hold for $Y = \Delta(x)$ to the expansion (51) shows that the function $A(X)$ accounts for the variation of the boundary layer thickness in the form

$$\Delta = \Delta_{00} - \epsilon^{2/3} \ell_{00}^{2/3} A(X) + \dots \quad (52)$$

In the critical case of vanishing γ the resulting problem consisting of Eqs. (44)–(47) has the “trivial” solution $\bar{\Psi} \equiv F_-(\bar{Y})$, giving $A \equiv 0$. However, for $\gamma \neq 0$ it has to be solved numerically. The corresponding solutions are plotted in figure 3 on page 9 (b): Exponential branching for $X \rightarrow -\infty$ is found as a consequence of Eq. (47), which reflects a match with the oncoming flow expressed by Eq. (31) and Eq. (33), for both the quantities \bar{U}_s and $A(X)$. In the sub-critical case $\gamma < 0$ the solution admits the non-trivial downstream-state

$$X \rightarrow \infty, \bar{Y} \rightarrow \infty: \bar{\Psi} X^{-5/6} \rightarrow F_+(\eta), \quad \eta = \bar{Y}/X^{1/3} = O(1), \quad (53)$$

which implies

$$X \rightarrow \infty: A(X) \sim A_+ X^{1/3}, \quad \bar{U}_s \sim U_+ X^{1/2}. \quad (54)$$

Equations (53) and (54) formally provide a match with the expansions (21), supplemented with Eq. (25), and (29) if s is replaced by \hat{s} there. In the latter representation these expansions are valid in the flow regime I_+ where $0 > s = O(\epsilon)$, see figure 4 on page 11.

It is important to note that the existence of perturbations of the non-trivial solution can be demonstrated which are due to linearization and indeed vanish in the limit $X \rightarrow \infty$. This suggests that this specific solution effectively provides a final downstream state of the flow rather than an isolated local solution. However, as the asymptotic analysis turns out to be rather lengthy in its details, that issue will be addressed separately in a subsequent paper.

D. The Goldstein-Type Singularity

For super-critical conditions $\gamma > 0$ the solution breaks down at a distinct location $X = X_G$, i.e. $x = x_G$ in the original scaling, see figure 3 on page 9. Again, this behavior is studied by means of a local similarity analysis, where a more detailed description of the associated multi-layered asymptotic structure of the local flow is presented in Ref. 22.

Introducing appropriate local variables

$$S = X - X_G, \quad \check{\eta} = \bar{Y}/(-S)^{1/3}, \quad \bar{f} = \bar{\Psi}/(-S)^{5/6}, \quad (55)$$

the stream function is expanded according to

$$\bar{f} = \bar{f}_0(\check{\eta}) + (-S)^r \bar{f}_1(\check{\eta}) + (-S)^{2r} \bar{f}_2(\check{\eta}) + \dots, \quad r > 0, \quad S \rightarrow 0_-, \quad (56)$$

where

$$1/2 \bar{f}_0'^2 - 5/6 \bar{f}_0 \bar{f}_0'' = 1 - (\bar{f}_0'')', \quad \check{\eta} = 0: \bar{f}_0 = \bar{f}_0'' = 0, \quad (57)$$

cf. Eq. (22). On condition that \bar{f}_0 has to exhibit sub-exponential growth as $\check{\eta} \rightarrow \infty$, an analytical investigation of Eq. (57) shows that this problem has two solutions, namely $\bar{f}_0 = F_-(\check{\eta})$ and

$$\bar{f}_0 = \sqrt{2} \check{\eta}. \quad (58)$$

However, only the latter solution provides a singular behavior as $S \rightarrow 0_-$. It predicts an Eulerian flow state, since the Reynolds shear stress vanishes in leading order. As a consequence,

$$\bar{U}_s \sim \sqrt{-2S}, \quad U_s \sim \sqrt{P_{00}(x_G - x)}, \quad x - x_G \rightarrow 0_-. \quad (59)$$

The local variations of, respectively, U_s and \bar{U}_s are displayed in figure 3 on page 9 as thin solid lines.

Since Eqs. (56) and (58) cannot be matched to the profile $\bar{\Psi}(X_G, \bar{Y})$ in region II, see figure 4 on page 11, a transitional flow regime has to be taken into account where the pressure gradient balances the inertia terms

and $\bar{Y}/(-S)^{1/6} = O(1)$. As a consequence, this further region, which is not encountered in the analysis of the marginal-separation singularity outlined in § III.B, then is found to include the sublayer where $\check{\eta} = O(1)$ considered here.²² Matching with the near-wall flow gives $r = 1/4$, and, in turn, $\bar{f}_1 \propto \check{\eta}^{5/2}$. Likewise, the matching procedure with respect to the flow regime II in the limit $S \rightarrow 0_-$ shows that

$$\begin{aligned} A - A_G &= O((-S)^{1/6}), \\ \Delta - \Delta_G &= O((x_G - x)^{1/6}) \quad \text{as } x - x_G \rightarrow 0_-, \end{aligned} \quad (60)$$

as indicated by the numerical solutions presented in figure 3 on page 9.

Solution (58) and the associated square-root behavior given by Eq. (59) has already been found by Melnik,^{24,25} but not in the context of marginally separated flow. It provides the analogon to the famous Goldstein singularity in laminar boundary layer theory.^{18,28,29}

We note that a Goldstein-type singularity appears quite naturally by evaluating Eqs. (8) and (9) at $Y = 0$, which gives

$$U_s dU_s/dx \sim -P_{00} + \partial T/\partial Y, \quad Y = 0, \quad x - x_G \rightarrow 0_-. \quad (61)$$

In turn, a local square-root behavior of U_s in $x - x_G$ is suggested in general whereas the marginal singularity characterized by the behavior (28) is seen to be a special case.²⁵ These results are essentially based upon the observation that Ψ and, thus, both T and $\partial T/\partial Y$ approach finite limits as $s \rightarrow 0$ and $S \rightarrow 0_-$, respectively. However, the rather surprising fact that in case of the square-root singularity $\partial T/\partial Y$ does not come into play at $S = Y = 0$ follows from the analysis of the locally self-similar behavior as expressed by Eq. (57).

IV. Local Interaction Theory for Marginally Separated Flows

In the following it is demonstrated how, by taking into account the locally strong interaction process between the boundary layer and the external bulk flow, the weak Goldstein-type singularity is eliminated and a uniformly valid description of the flow with respect to the Reynolds equations (3), (4) is achieved. More precisely, it is pointed out that the locally induced pressure gradient, which is not given in advance but rather to be determined simultaneously together with the flow inside the boundary layer, must enter the analysis if $\epsilon = O(\alpha^{3/10})$ or smaller. Since nonlinear convective effects can not be neglected even near the surface, this procedure results in a triple-deck problem which, therefore, clearly differs from the formulation of laminar marginal separation^{19,20} but is related to laminar short-scale boundary layer interaction theory.^{21,33}

Note that the elliptic nature of the equations determining the induced potential flow requires the existence of a boundary layer solution which does not terminate in a Goldstein singularity. Consequently, we at first assume that $\gamma \leq 0$. However, the resulting interaction theory is *a posteriori* readily seen to apply to flows having $\gamma > 0$ also.

We furthermore stress that inspection of the equations of motion (3) and (4) indicates that the pressure gradient normal to the surface as well as the Reynolds normal stresses are negligibly small in any of the flow regimes considered in the subsequent investigation and will, therefore, be disregarded.

A. Induced Potential Flow

We now consider the boundary layer solutions, assuming that $\epsilon \ll 1$, from the viewpoint of the external free-stream flow which is considered to be irrotational at least up to $O(\alpha)$ since the Reynolds stresses are of $o(\alpha)$ there. That is, in the double limit $\epsilon \rightarrow 0$, $\alpha \rightarrow 0$ the stream function and the pressure are expanded in the form

$$q = q_{00}(\hat{s}, y) + \epsilon q_{01}(\hat{s}, y) + \dots + \alpha [q_{10}(\hat{s}, y) + \epsilon q_{11}(\hat{s}, y) + \dots] + O(\alpha^2), \quad q = \psi, p, \quad (62)$$

according to the expansions (14) and (31). The coordinate shift provided by Eq. (41) ensures that the sub-expansion in terms of powers of ϵ of the expansion (62) only accounts for the Taylor expansion of u_e around $\hat{s} = 0$. The terms of $O(\alpha)$ reflect the streamline displacement caused by the boundary layer. Then the stream functions ψ_{00} and ψ_{10} satisfy Laplace's equation

$$\frac{\partial}{\partial \hat{s}} \left(\frac{1}{h} \frac{\partial \psi_{1i}}{\partial \hat{s}} \right) + \frac{\partial}{\partial y} \left(h \frac{\partial \psi_{1i}}{\partial y} \right) = 0, \quad i = 0, 1, \quad (63)$$

subject to the boundary conditions

$$\psi_{00}(\hat{s}, 0) = 0, \quad \psi_{10}(\hat{s}, 0) = \Psi_0(\hat{x}, \Delta_0(\hat{x})) - \Delta_0(\hat{x})U_0(\hat{x}). \quad (64)$$

Equation (64) follows from patching the stream function at the boundary layer edge up to $O(\alpha)$ by means of a Taylor expansion about $y = 0$, taking into account Eq. (41), and the relationship

$$u_e(x) = U_0(\hat{x}) = \frac{\partial \psi_{00}}{\partial y}(\hat{s}, 0). \quad (65)$$

Hence, ψ_{10} is seen to be determined uniquely in a certain domain $y \geq 0$ and can, in principle, be calculated by adopting standard methods. In turn, the induced pressure disturbance p_{10} follows from evaluating the linearized Bernoulli's law,

$$p_{10} = \frac{1}{h^2} \frac{\partial \psi_{00}}{\partial \hat{s}} \frac{\partial \psi_{10}}{\partial \hat{s}} - \frac{\partial \psi_{00}}{\partial y} \frac{\partial \psi_{10}}{\partial y}. \quad (66)$$

We note that, without any loss of generality, in Eq. (66) any remaining pressure perturbation for vanishing velocity variations is discarded.

It is evident from inspection of Eq. (64) and the foregoing analysis of the marginally separating boundary layer solution Ψ_0, Δ_0 that ψ_{10} and p_{10} behave regularly except for the location $\hat{s} = y = 0$. By defining the limiting value

$$\psi_{100} = \psi_{10}(0, 0) = \Psi_{00}(\Delta_{00}) - \Delta_{00}U_{00}, \quad (67)$$

which is a quantity of $O(1)$, a regular upstream but singular downstream behavior of ψ_{10} in the limit $y = 0, \hat{s} \rightarrow 0$ is found,

$$\hat{s} \rightarrow 0_- : \quad \psi_{10}(\hat{s}, 0) - \psi_{100} = O(\hat{s}), \quad (68)$$

$$\hat{s} \rightarrow 0_+ : \quad \frac{\psi_{10}(\hat{s}, 0) - \psi_{100}}{\ell_{00}^{2/3} U_{00}} \sim A_+ \hat{s}^{1/3}. \quad (69)$$

These conditions are rich enough to contain the associated singular local behavior of the pressure perturbation p_{10} . A local analysis of Eq. (63) supplemented with Eqs. (64) and (65) shows that

$$\psi_{00}/U_0(\hat{x}) = y - k(\hat{x})y^2/2 + O(y^3) \quad \text{as } y \rightarrow 0_+, \quad (70)$$

and

$$\frac{\psi_{10} - \psi_{100}}{\ell_{00}^{2/3} U_{00}} \sim A_+ \rho^{1/3} g(\vartheta), \quad \vartheta = \arctan(y/\hat{s}), \quad \pi \geq \vartheta \geq 0, \quad \text{as } \rho = \sqrt{\hat{s}^2 + y^2} \rightarrow 0, \quad (71)$$

where

$$g'' + g/9 = 0, \quad g(\pi) = 0, \quad g(0) = 1. \quad (72)$$

The solution of this problem is given by

$$g(\vartheta) = \cos(\vartheta/3) - \sin(\vartheta/3)/\sqrt{3}. \quad (73)$$

Substituting Eq. (70) evaluated for $\hat{s} \rightarrow 0$, Eq. (71), and Eq. (73) into Eq. (66) then yields

$$\frac{p_{10}}{\ell_{00}^{2/3} U_{00}^2} \sim A_+ \rho^{-2/3} \left[\frac{\cos(2\vartheta/3)}{3\sqrt{3}} - \frac{\sin(2\vartheta/3)}{3} \right]. \quad (74)$$

Finally, one obtains

$$\hat{s} \rightarrow 0_- : \quad \frac{p_{10}(\hat{s}, 0)}{\ell_{00}^{2/3} U_{00}^2} \sim -\frac{2A_+}{3\sqrt{3}} \hat{s}^{-2/3}, \quad (75)$$

$$\hat{s} \rightarrow 0_+ : \quad \frac{p_{10}(\hat{s}, 0)}{\ell_{00}^{2/3} U_{00}^2} \sim \frac{A_+}{3\sqrt{3}} \hat{s}^{-2/3}. \quad (76)$$

Again, Eqs. (68), (69) and (75), (76) agree exactly with the behavior of the irrotational flow near the trailing edge of a flat plate which is induced by the laminar Blasius boundary layer and the near wake. The close

relationship between these two different flow configurations arising from the similarity structure of the shear layer downstream of the singular point will also be evident in the resulting interaction problem to be derived subsequently.^{21, 34, 35}

The local singularity in the induced potential flow given by Eqs. (71) and (74) indicates a breakdown of the expansions (62) for $\rho \rightarrow 0_+$ as one expects from the strong streamwise variations on a length scale of $O(\epsilon^2)$ of the flow inside the boundary layer discussed in § III. As already mentioned, the higher-order contributions q_{11}, \dots to the expansions Eq. (62) do not behave more singularly. Therefore, the singularity in p_{10} represented by Eqs. (75), (76) and the associated response of the boundary layer flow suffice to determine the scalings of the adjustment regions which will account for an uniformly valid flow description.

B. A Triple-Deck Problem for Turbulent Boundary Layers

As in the following also the effect of the induced pressure on the boundary layer is necessarily taken into account, this section provides a revision of § III.C.2. Therefore, the expansions of the quantities differ in the corresponding details. That is, here an asymptotically correct analysis of the problem is carried out in line with the set of the full Reynolds equations Eqs. (3), (4) rather than their boundary layer approximation given by Eqs. (8) and (9). By dealing with second-order boundary layer theory, however, the local perturbations in the boundary layer triggered by the behavior of the induced pressure p_{10} given by Eqs. (74)–(76) are considered first.

In the limit $\hat{s} \rightarrow 0$ the stream function in the boundary layer where $Y = O(1)$ is given by $\psi \sim \alpha \Psi_{00}(Y)$, see Eqs. (16) and (51). We now seek the perturbations there owing to the induced pressure p_{10} upstream and downstream of $\hat{s} = 0$. Inspection of the momentum equation (3) in combination with the near-wall behavior given by Eq. (24) then shows that the disturbances caused by the pressure gradient $\partial p_{10}/\partial \hat{s}$ of both the Reynolds shear stress gradient and the inertia terms balance in, respectively, the regions I_- and I_+ , see figure 5 on the following page, where the wall coordinate

$$\hat{\eta} = Y/(\ell_{00}^{2/3} |\hat{s}|^{1/3}) \quad (77)$$

is a quantity of $O(1)$. There, the following expansions are suggested in the triple limit $\epsilon \rightarrow 0$, $\alpha \rightarrow 0$, $\hat{s} \rightarrow 0$ both for

$$\begin{aligned} \hat{s} \rightarrow 0_- : \quad \frac{\psi}{\ell_{00}^{2/3} P_{00}^{1/2}} &= \alpha \left[(-\hat{s})^{5/6} F_-(\hat{\eta}) + (-\hat{s})^{1/3} (\epsilon - B\hat{s}) \hat{\eta} + (-\hat{s})^{4/3} \frac{B}{180} \hat{\eta}^4 + \dots \right] \\ &+ \alpha^2 (-\hat{s})^{-5/6} \frac{\ell_{00}^{2/3} U_{00}^2}{P_{00}} G_-(\hat{\eta}) + \dots, \\ \frac{p - p_0(x_0)}{P_{00}} &= \hat{s} + \dots - \alpha (-\hat{s})^{-2/3} \frac{2A_+}{3\sqrt{3}} \frac{\ell_{00}^{2/3} U_{00}^2}{P_{00}} + \dots, \end{aligned} \quad (78)$$

and for

$$\begin{aligned} \hat{s} \rightarrow 0_+ : \quad \frac{\psi}{\ell_{00}^{2/3} P_{00}^{1/2}} &= \alpha \hat{s}^{5/6} F_+(\hat{\eta}) + \dots + \alpha^2 \hat{s}^{-5/6} \frac{\ell_{00}^{2/3} U_{00}^2}{P_{00}} G_+(\hat{\eta}) + \dots, \\ \frac{p - p_0(x_0)}{P_{00}} &= \hat{s} + \dots + \alpha \hat{s}^{-2/3} \frac{A_+}{3\sqrt{3}} \frac{\ell_{00}^{2/3} U_{00}^2}{P_{00}} + \dots. \end{aligned} \quad (79)$$

In the expansions (78) and (79) the exponentially growing terms considered in § III.C, which cause a breakdown when $\hat{s} = O(\epsilon^2)$, are represented by dots. This is sufficient as we now rather focus on the perturbations proportional to α which are responsible for the onset of the interaction process of the flow upstream and downstream of the interaction region, cf. figure 5 on the next page.

Inserting expansions (78) and (79) into Eq. (3) and rearranging terms up to $O(\alpha |\hat{s}|^{-5/3})$ gives rise to a linear inhomogeneous third-order problem for $G_{\mp}(\hat{\eta})$,

$$\pm 2(F_{\mp}'' G_{\mp}'')' - \frac{5}{6} F_{\mp} G_{\mp}'' - \frac{2}{3} F_{\mp}' G_{\mp}' + \frac{5}{6} F_{\mp}'' G_{\mp} = (-1 \mp 3) \frac{A_{\pm}}{9\sqrt{3}}, \quad G_{\mp}(0) = G_{\mp}''(0) = 0, \quad (80)$$

where the upper and the lower signs correspond to the upstream and the downstream case, respectively.

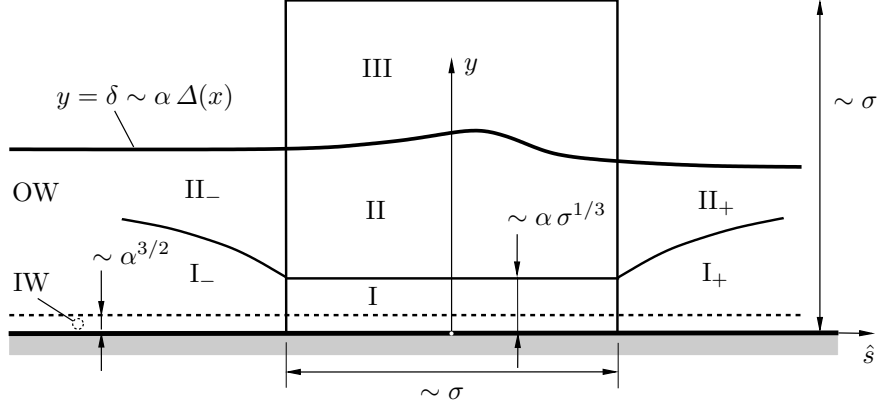


Figure 5. Asymptotic splitting of the flow in the formal limit $Re^{-1} = 0$ due to the interaction process of the oncoming (subscripts $-$) and downstream evolving (subscripts $+$) boundary layer (outer wake OW, inner wake IW, see §II.B.2), triple-deck structure (lower deck I, main deck II, upper deck III).

1. Upstream Onset of the Interaction Process

In the upstream case the problem (80) assumes the form

$$(\hat{\eta}^{1/2} G_-''')' - \frac{1}{9} \hat{\eta}^{5/2} G_-'' - \frac{2}{9} \hat{\eta}^{3/2} G_-' + \frac{5}{12} \hat{\eta}^{1/2} G_- = -\frac{2A_+}{9\sqrt{3}}, \quad G_-(0) = G_-''(0) = 0. \quad (81)$$

By applying the transformation

$$G_-(\hat{\eta}) = F'_-(\hat{\eta}) \left[\int_0^{\hat{\eta}} \frac{H(z) - H(0)}{\zeta^{3/2}} d\zeta - 2 \frac{H(0)}{\hat{\eta}^{1/2}} \right], \quad z = \frac{\zeta^3}{27}, \quad (82)$$

Eq. (81) is conveniently cast into an inhomogeneous Kummer's equation³⁶ for $H(z)$,

$$zH'' + (4/3 - z)H' - 7/6 H = -A_+/9 z^{-1/2} \quad (83)$$

where the boundary conditions in Eq. (81) require H to be bounded for $z \rightarrow 0$. In addition, the third boundary condition for G_- missing in Eq. (81) follows from the requirement that H clearly must not grow exponentially for $z \rightarrow \infty$. The solution of (83) is found in terms of a hypergeometric series which, by using the integral representation of the Beta function,³⁶ can be expressed in closed form as an integral. After some manipulations we obtain

$$H(z) = \frac{A_+}{9} \frac{\pi}{2^{2/3} \Gamma(1/6) \Gamma(4/3)} \int_0^1 \frac{t^{1/6} e^{zt} \operatorname{erfc}(\sqrt{zt})}{(1-t)^{5/6}} dt. \quad (84)$$

Inserting Eq. (84) into Eq. (82) then yields the limiting behavior of $G_-(\hat{\eta})$,

$$G_-'(0) = -A_+ \frac{\sqrt{\pi}}{3\sqrt{3}} \quad (85)$$

and

$$G_- = A_- F'_-(\hat{\eta}) [1 + O(\hat{\eta}^{-2})] \quad \text{as } \hat{\eta} \rightarrow \infty, \quad (86)$$

where

$$A_- = \int_0^\infty \frac{H(z) - H(0)}{3^{3/2} z^{7/6}} dz = -A_+ \frac{2^{7/3} \Gamma(5/6) \sqrt{\pi}}{27}. \quad (87)$$

We now consider the effect of the induced pressure on the surface slip velocity u_s which is defined by

$$u_s = \partial\psi/\partial y \quad \text{at } y = 0. \quad (88)$$

For distances $\hat{s} = O(1)$, the surface slip is primarily given by the boundary layer solution, i.e.

$$u_s = U_s(x) + \dots \quad (89)$$

Here the dots denote higher order terms due to finite values of ϵ and α . In the triple limit $\alpha \rightarrow 0$, $\epsilon \rightarrow 0$, $\hat{s} \rightarrow 0_-$ evaluation of Eq. (78) gives

$$\frac{u_s}{P_{00}^{1/2}} = \epsilon - B\hat{s} + \dots + \alpha(-\hat{s})^{-7/3} \frac{\ell_{00}^{2/3} U_{00}^2}{P_{00}} G'_-(0) + \dots, \quad (90)$$

where the first terms on the right-hand side represent the expansion of $U_s(x)$ about $x = x_0$, using Eq. (41). Equation (90) allows for an appealing physical interpretation: as indicated by Eqs. (78) and (85), the negative (favorable) induced pressure gradient upstream of $\hat{s} = 0$ causes a deceleration of the flow close to the surface. This rather surprising phenomenon has not been observed yet in laminar boundary layer flows. Here, however, it originates from the fact that convection does not vanish at the surface.

Finally, matching of the expansions (78) and (79) with the flow in the boundary layer main regimes Π_- and Π_+ (figure 5 on the preceding page) where $Y = O(1)$ demonstrates, by noticing Eq. (86), that the expansions of the stream function there take on the form

$$\hat{s} \rightarrow 0_- : \quad \psi = \alpha [\Psi_{00}(Y) + (\epsilon - B\hat{s})\Psi_{01}(Y) + \dots] + \alpha^2(-\hat{s})^{-4/3} \frac{\ell_{00}^{4/3} U_{00}^2}{P_{00}} A_- \Psi'_{00}(Y) + \dots, \quad (91)$$

$$\hat{s} \rightarrow 0_+ : \quad \psi = \alpha [\Psi_{00}(Y) + \hat{s}^{1/3} \ell_{00}^{2/3} A_+ \Psi'_{00}(Y) + \dots] + \alpha^2 \hat{s}^{-4/3} \frac{\ell_{00}^{4/3} U_{00}^2}{P_{00}} C_+ \Psi'_{00}(Y) + \dots. \quad (92)$$

It is anticipated in Eq. (92) that, in analogy to Eq. (86), the function G_+ behaves as $G_+(\hat{\eta}) \sim C_+ F'_+(\hat{\eta} + A_+)$, $\hat{\eta} \rightarrow \infty$, with some constant C_+ . For this mathematical detail the reader is again referred to a future publication.

2. Main Deck

A breakdown of the asymptotic structure considered so far occurs due to both the exponentially growing eigensolutions when $\hat{s} = O(\epsilon^2)$, see the expansion (31) and Eq. (41), and the singular induced pressure gradient $\partial p_{10}/\partial \hat{s}$ when $\hat{s} = O(\alpha^{3/5})$, cf. the expansions (91) and (92) above. To take into account both causes of non-uniformness, we consider a distinguished limit by introducing the coupling parameter

$$\chi = \frac{\epsilon^{10/3}}{\alpha} \frac{P_{00}}{\ell_{00}^{2/3} U_{00}^2}, \quad (93)$$

which is required to be of $O(1)$ in the double limit $\epsilon \rightarrow 0$, $\alpha \rightarrow 0$. Then the streamwise distance where the expansions (91), and (92) cease to be valid is found to be measured by

$$\hat{s} = \sigma \hat{X}, \quad \sigma = (\epsilon/\Gamma)^2 \quad \text{with} \quad 0 \leq \Gamma \leq 1, \quad (94)$$

which in turn redefines the streamwise extent of the main deck (region II in figure 5 on the previous page). Here the parameter Γ is introduced to provide a bijective function $\chi(\Gamma)$ having the properties

$$\chi'(\Gamma) > 0, \quad \chi_b = \chi(1) \leq \infty, \quad \chi = O(\Gamma^{10/3}) \quad \text{as} \quad \Gamma \rightarrow 0, \quad (95)$$

where the upper bound χ_b of the coupling parameter may be chosen arbitrarily. It is convenient with respect to the subsequent analysis to specify the relationship between Γ and χ by the definition of a further function $\Lambda(\Gamma)$ in the form

$$\chi(\Gamma) = \Gamma^{10/3} / \Lambda(\Gamma), \quad \Lambda'(\Gamma) \leq 0. \quad (96)$$

Then Λ is seen to be bounded, and

$$\Lambda(0) > \Lambda(1) = 1/\chi_b. \quad (97)$$

From Eqs. (93), (94) and (96) one then readily concludes that

$$\epsilon = \sigma^{1/2} \Gamma, \quad \alpha = \sigma^{5/3} \Lambda \frac{P_{00}}{\ell_{00}^{2/3} U_{00}^2}. \quad (98)$$

The meaning of Eqs. (93)–(98) is the following: The case $\chi_b = \infty$ or, equivalently, $\Lambda(1) = 0$, recovers the pure boundary layer limit, that is $\alpha = 0$ for finite values of ϵ , already discussed in §III.C.2, where the induced pressure gradient does not come into play at all. On the other hand, the limit $\chi = 0$ refers to the case $\gamma = \epsilon = 0$ where $\sigma = O(\alpha^{3/5})$. These considerations imply that the regions I, II, and III, as sketched in figure 5 on page 18, are located a distance of $O(\epsilon)$ upstream of the position of the marginal singularity given by $s = 0$, cf. Eq. (41), where the lower and upper limits of the magnitude of their streamwise extent are given by $O(\alpha^{3/5})$ and $O(\epsilon^2)$, respectively.

Inspection of Eqs. (91) and (92) indicates that, in the main-deck region, the expansions (51) and (52) now take on the asymptotically correct forms

$$\psi/\alpha = \Psi_{00}(Y) + \sigma^{1/3} \ell_{00}^{2/3} \hat{A}(\hat{X}) \Psi'_{00}(Y) + \dots + (\sigma^{1/2} \Gamma - \sigma B \hat{X}) \Psi_{01}(Y) + \dots \quad (99)$$

and

$$\delta/\alpha = \Delta_{00} - \sigma^{1/3} \ell_{00}^{2/3} \hat{A}(\hat{X}) + \dots \quad (100)$$

in the limit $\sigma \rightarrow 0$. Here and in the following the substitutions given by Eq. (98) have been applied. Moreover, the expansions (78) and (79) imply that the pressure in the main deck can be written as

$$p = p_0(x_0) + \sigma P_{00}[\hat{X} + \Lambda \hat{P}(\hat{X})] + \dots \quad (101)$$

Both the displacement function $\hat{A}(\hat{X})$ and the pressure function $\hat{P}(\hat{X})$ are quantities of $O(1)$ and unknown at this stage of the analysis. However, matching with the regions II_- and II_+ reveals the following asymptotes,

$$\hat{X} \rightarrow -\infty : \hat{A}(\hat{X}) \sim \Lambda A_- \hat{X}^{-4/3}, \quad (102)$$

$$\hat{P}(\hat{X}) \sim -\frac{2A_+}{3\sqrt{3}} \hat{X}^{-2/3}, \quad (103)$$

$$\hat{X} \rightarrow +\infty : \hat{A}(\hat{X}) \sim A_+ \hat{X}^{1/3}, \quad (104)$$

$$\hat{P}(\hat{X}) \sim \frac{A_+}{3\sqrt{3}} \hat{X}^{-2/3}. \quad (105)$$

3. Upper Deck

The above considerations suggest that the expansion (62) of the flow in the external regime where \hat{s} and y are quantities of $O(1)$ fail in the upper deck (region III in figure 5 on page 18). There appropriately rescaled variables are given by the scalings (94) and

$$y = \sigma \hat{y}, \quad \hat{y} = O(1). \quad (106)$$

The singular behavior of the stream function and the pressure expressed by Eqs. (69), (75), and (76) then gives rise to the expansions

$$\psi = \sigma U_{00} \hat{y} + \dots + \Lambda \frac{P_{00}}{U_{00}} \left[\sigma^{5/3} \frac{\Psi_{100}}{\ell_{00}^{2/3} U_{00}} + \sigma^2 \hat{\psi}(\hat{X}, \hat{y}) + \dots \right], \quad (107)$$

$$p = p_0(x_0) + \sigma P_{00}[\hat{X} + \Lambda \hat{p}(\hat{X}, \hat{y})] + \dots \quad (108)$$

Here terms proportional to Λ represent the potential flow induced locally by the boundary layer displacement.

The pressure \hat{p} is calculated from Bernoulli's law, cf. Eq. (66), which by balancing terms up to $O(\sigma^2)$ reduces to

$$\hat{p} = -\frac{\partial \hat{\psi}}{\partial \hat{y}}, \quad (109)$$

and the stream function $\hat{\psi}$ is seen to satisfy the Cauchy problem

$$\frac{\partial^2 \hat{\psi}}{\partial \hat{X}^2} + \frac{\partial^2 \hat{\psi}}{\partial \hat{y}^2} = 0, \quad \hat{\psi}(\hat{X}, 0) = \hat{A}(\hat{X}), \quad \hat{\psi} \sim A_+ \hat{\rho}^{1/3} g(\vartheta) \quad \text{as} \quad \hat{\rho} = \sqrt{\hat{X}^2 + \hat{y}^2} \rightarrow \infty. \quad (110)$$

Herein ϑ is given by Eq. (71) where the ratio y/\hat{s} is to be replaced by \hat{y}/\hat{X} according to the local scaling provided by Eqs. (106) and (94). The boundary conditions in Eq. (110) follow from patching the stream

function at the boundary layer edge by using Eqs. (99), (100) and from a match of $\hat{\psi}$ with the singular behavior of ψ_{10} given by Eq. (71), respectively. In turn, \hat{p} matches the asymptotic behavior of p_{10} as expressed by Eqs. (74)–(76). Additionally, comparing Eq. (108) with Eq. (101) and taking into account Eq. (109) yields the relationship

$$\frac{\partial \hat{\psi}}{\partial \hat{y}}(\hat{X}, 0) = -\hat{P}(\hat{X}) \quad (111)$$

where $\hat{P}(\hat{X})$ is seen to be the induced surface pressure. Consequently, and as a well-known result from potential theory,³³ $\hat{P}(\hat{X})$ and $-\hat{A}'(\hat{X})$ form a Hilbert pair, i.e.

$$\{\hat{P}(\hat{X}), -\hat{A}'(\hat{X})\} = \frac{1}{\pi} \oint_{-\infty}^{\infty} \frac{\{\hat{A}'(\hat{S}), \hat{P}(\hat{S})\}}{\hat{X} - \hat{S}} d\hat{S}. \quad (112)$$

4. Lower Deck

The analysis is finalized by considering the flow in the lower deck (region I in figure 5 on page 18) in the limit $\sigma \rightarrow 0$. Hence, we introduce rescaled local variables \hat{Y} , $\hat{\Psi}$ of $O(1)$ according to

$$\frac{Y}{\ell_{00}^{2/3}} = \sigma^{1/3} \hat{Y}, \quad \frac{\psi}{\ell_{00}^{2/3} P_{00}^{1/2}} \sim \alpha \sigma^{5/6} \hat{\Psi}(\hat{X}, \hat{Y}). \quad (113)$$

Moreover, the pressure is given by Eq. (101). The leading-order problem governing the flow in the lower deck is found by inserting these quantities into the equations of motion (3) and (4) or, equivalently, by applying the transformation

$$\hat{X} = \Gamma^2 X, \quad \hat{Y} = \Gamma^{2/3} \bar{Y}, \quad \hat{\Psi} = \Gamma^{5/3} \bar{\Psi} \quad (114)$$

to Eq. (43). As a result, the inclusion of the induced pressure gradient in Eq. (44) is seen to be sufficient to generate an asymptotically correct description of the flow near the surface. The lower-deck equations then read

$$\frac{\partial \hat{\Psi}}{\partial \hat{Y}} \frac{\partial^2 \hat{\Psi}}{\partial \hat{X} \partial \hat{Y}} - \frac{\partial \hat{\Psi}}{\partial \hat{X}} \frac{\partial^2 \hat{\Psi}}{\partial \hat{Y}^2} = -1 - \Lambda(\Gamma) \hat{P}'(\hat{X}) + \frac{\partial \hat{T}}{\partial \hat{Y}}, \quad \hat{T} = \frac{\partial^2 \hat{\Psi}}{\partial \hat{Y}^2} \Big|_{\frac{\partial^2 \hat{\Psi}}{\partial \hat{Y}^2}}. \quad (115)$$

They are subject to the boundary conditions

$$\hat{Y} = 0: \quad \hat{\Psi} = \hat{T} = 0, \quad (116)$$

$$\hat{Y} \rightarrow \infty: \quad \hat{T} - \hat{Y} \rightarrow \hat{A}(\hat{X}), \quad (117)$$

$$\hat{X} \rightarrow -\infty: \quad \hat{\Psi} \rightarrow F_-(\hat{Y}) + \Gamma \hat{Y}, \quad 0 \leq \Gamma \leq 1, \quad (118)$$

$$\hat{X} \rightarrow \infty, \hat{Y} \rightarrow \infty: \quad \hat{\Psi} \hat{X}^{-5/6} \rightarrow F_+(\hat{\eta}), \quad \hat{\eta} = \hat{Y}/\hat{X}^{1/3} = O(1). \quad (119)$$

The conditions (118), (119), and (117) follow from a match with the expansions (78), (79), and (99), respectively, which clearly cease to be valid in the lower-deck flow regime. The asymptotic behavior expressed by relationship (117), however, can be shown to be determined by the upstream initial condition (118) rather than provide an additional boundary condition to be imposed. Most important, since both the functions $\hat{P}(\hat{X})$ and $\hat{A}(\hat{X})$ are seen to be part of the solution, Eqs. (115)–(119) have to be supplemented with one of the relationships given by Eq. (112) in order to complete the triple-deck problem.

This fundamental problem which governs turbulent marginal separation associated with the triple-deck scheme outlined above has the following important properties:

- (i) As a highly remarkable characteristic not known in laminar triple-deck theory at present (apart from a laminar supersonic triple-deck flow model proposed by Lipatov³⁷), the lower-deck equations (115) include both the (locally constant) imposed and the induced streamwise pressure gradient given by $\Lambda \hat{P}'(\hat{X})$.
- (ii) A property also not observed in subsonic laminar interacting boundary layers so far is that turbulent marginal separation is linked to the existence of eigensolutions of the underlying triple-deck problem. In this connection we note that Eqs. (115)–(119) and Eq. (112) allow for the “trivial” solution $\hat{\Psi} = F_-(\hat{Y}) + \Gamma \hat{Y}$, $\hat{A}(\hat{X}) = \hat{P}(\hat{X}) = 0$. However, a non-trivial solution is conveniently enforced by prescribing the downstream condition (119). Therefore, the ellipticity of the triple-deck problem is not

only due to the imposed pressure gradient, cf. Eq. (112), but also arises from the non-trivial downstream state as expressed by Eq. (119) and in agreement with Eq. (53).

- (iii) It is inferred from Eq. (96) that the triple-deck solutions depend on χ solely, independent of the specific choice of the function $\Lambda(\Gamma)$. This is also expressed by the invariance properties

$$\begin{aligned}\hat{\Psi}(\hat{X}, \hat{Y}) &= \lambda^{-5/6} \hat{\Psi}(\mathcal{X}, \mathcal{Y}), \quad \hat{A}(\hat{X}) = \lambda^{-1/3} \hat{A}(\mathcal{X}), \quad \hat{P}(\hat{X}) = \lambda^{2/3} \hat{P}(\mathcal{X}), \\ \mathcal{X} &= \lambda(\hat{X} - \mu), \quad \mathcal{Y} = \lambda^{1/3} \hat{Y},\end{aligned}\tag{120}$$

satisfied by the solution $\hat{\Psi}$, \hat{A} , \hat{P} for a given value of χ . Here \hat{X} is stretched by an arbitrary factor $\lambda > 0$. The real parameter μ corresponds to an origin shift in \hat{X} of the solution. However, the ambiguity of the solution expressed by that translation invariance has to be eliminated by the exponentially decreasing eigensolutions occurring upstream, giving

$$\hat{\Psi} = F_-(\hat{Y}) + \Gamma \hat{Y} + \dots - \text{sgn}(\gamma) \Gamma^{5/3} f(\hat{Y}/\Gamma^{2/3}) \exp(\hat{X}/(3\Gamma^2)) + \dots, \quad \hat{X} \rightarrow -\infty.\tag{121}$$

This expansion follows directly from Eq. (47) by taking into account Eq. (114). Equation (121) states that, in definite contrast to the non-interactive case which is expressed by $\Gamma = 1$ and $\Lambda = 0$ or, equivalently, Eq. (44), the interaction process is insensitive to the sign of γ . The latter rather enters the triple-deck solution only via exponentially small terms. Their strength is fixed by the requirement of a match with the oncoming flow, which in turn eliminates the translation invariance of the solution by means of an adequate choice of the group parameter μ .

It is useful to introduce the rescaled surface slip velocity

$$\hat{U}_s = \frac{\partial \hat{\Psi}}{\partial \hat{Y}}(\hat{X}, 0).\tag{122}$$

A comparison with Eq. (90) gives

$$u_s \sim \sigma^{1/2} P_{00}^{1/2} \hat{U}_s \quad \text{as} \quad \hat{X} = O(1),\tag{123}$$

and by matching of Eq. (122) with Eq. (78) or, equivalently, Eq. (90), and Eq. (79) one recovers the expansions holding upstream and downstream, respectively,

$$\hat{X} \rightarrow -\infty: \quad \hat{U}_s \sim \Gamma - \Lambda G'_-(0) \hat{X}^{-7/6},\tag{124}$$

$$\hat{X} \rightarrow +\infty: \quad \hat{U}_s \sim U_+ \hat{X}^{1/2}.\tag{125}$$

The latter of these relationships reflects the match with the non-trivial self-similar solution expressed by $F_+(\hat{\eta})$. The asymptotic behavior (124) is seen to be valid for all admissible values of Γ and Λ and demonstrates the effect of both the exponentially decaying eigensolutions and of the induced pressure gradient on the triple-deck solution: The first determines the magnitude of the control parameter ϵ and, in turn, Γ , which fixes the upstream limit of the surface slip. The upstream deceleration of the flow, however, is primarily caused by the induced pressure gradient the strength of which is measured by Λ .

As a consequence of Eqs. (115) and (116), and by noting the definition (122), one obtains the near-wall asymptotes

$$\begin{aligned}\hat{\Psi} &= \hat{U}_s(\hat{X}) \hat{Y} + 4/15 \text{sgn}(\gamma) |\gamma|^{1/2} \hat{Y}^{5/2} + O(\hat{Y}^4), \quad \hat{T} = \gamma \hat{Y} + O(\gamma \hat{Y}^{5/2}, \hat{Y}^4), \\ \gamma(\hat{X}) &= \hat{U}_s(\hat{X}) \hat{U}'_s(\hat{X}) + 1 + \Lambda \hat{P}'(\hat{X}), \quad \hat{Y} \rightarrow 0.\end{aligned}\tag{126}$$

Furthermore, as already indicated by the asymptotic behavior (25) of the downstream similarity solution, for large values of \hat{Y} the solution is seen to be invariant with respect to a shift in \hat{Y} of the amount $\hat{A}(\hat{X})$. In other words, a non-vanishing value of A_+ enforces the non-trivial eigensolution of the triple-deck problem having $\hat{A} \neq 0$. On the other hand, one draws the conclusion that the possible shift is an immediate consequence of the hyperbolic convective operator giving rise to the predominating convective terms on the left-hand side

of the momentum balance in (115). By taking into account the upstream asymptotes given by Eq. (118) together with $\hat{P}(-\infty) = 0$, the analysis then yields

$$\begin{aligned}\hat{\Psi} &= F_-(\hat{Z}) + 3/4 \Lambda \hat{P} \hat{Z}^{-1/2} - 9/56 \Gamma \Lambda \hat{P} \hat{Z}^{-2} + \hat{Z}^{-7/2} \sum_{n=0}^{\infty} \Phi_n \hat{Z}^{-3n/2} + \text{TST}, \\ \hat{T} &= \hat{Z} + 9/8 \Lambda \hat{P} \hat{Z}^{-2} - 27/14 \Gamma \Lambda \hat{P} \hat{Z}^{-7/2} + \hat{Z}^{-5} \sum_{n=0}^{\infty} \Xi_n \hat{Z}^{-3n/2} + \text{TST}, \quad \hat{Z} = \hat{Y} + \hat{A} \rightarrow \infty.\end{aligned}\quad (127)$$

We note that the algebraic terms following the leading-order contributions in these asymptotic expansions vanish if and only if $\Lambda = 0$. To be more precise, both the leading-order coefficients Φ_0 and Ξ_0 in the remainder series are quantities of $O(\Lambda, \Lambda^2, \Lambda \Gamma^2)$. One also easily verifies the match of Eq. (127) with the higher-order contribution determined by $G_-(\hat{\eta})$ to the expansion (78), which characterizes the oncoming flow, in the limit $\hat{\eta} \rightarrow \infty$, see Eqs. (86), (87), and (102).

C. Numerical Results

1. Method

For the numerical treatment of the triple-deck problem posed by Eqs. (115)–(119) and Eq. (112) a carefully devised variable transform which maps the interval $-\infty < \hat{X} < \infty$ onto the range $[-1, 1]$ was performed in order to handle the singular upstream and downstream behavior at infinity in an efficient manner. In addition, also a coordinate stretching in \hat{Y} -direction was introduced which, among others, accounts for the far-field relationships given by Eq. (127), where only the terms larger than the remainder sums were regarded. Most important, however, it regularizes the half-power behavior $\hat{\Psi} = \hat{U}_s(\hat{X}) \hat{Y} + O(\hat{Y}^{5/2})$ for $\hat{Y} \rightarrow 0$, see Eq. (126), and thus allows for a higher resolution of the flow close to the surface. These ideas were put forward in its original form by Smith and Merkin,³⁸ see also Ref. 39 and Ref. 40. The thereby transformed equations were discretized on a uniformly spaced mesh by approximating all derivatives using central finite-differences with second-order accuracy. Therefore, the elliptic character of the problem is fully retained. The stream function $\hat{\Psi}$ and the pressure \hat{P} served as the only dependent variables. The resulting system of nonlinear algebraic equations was solved directly by adopting a modification of the Powell hybrid method⁴¹ where the Jacobians are calculated numerically in principle but, whenever feasible, updated by means of a secant approximation during the Newton iteration. In each Newton step, the resulting linear system of equations are solved by advantageously exploiting the sparsity pattern of the Jacobian. Under reasonable conditions this algorithm guarantees a fast rate of global convergence. We note that typically a grid of 300 points in \hat{X} -direction and 150 points in \hat{Y} -direction was employed where the principal limit of resolution depends on the hardware memory available. The stopping criterion for the iteration process was provided by the machine-dependent optimal accuracy of the solution. It should be stressed that the indeterminacy of the solutions with respect to a shift of the origin, expressed by Eq. (120) and discussed in (iii) above, is eliminated numerically as a consequence of the discretization process. A more detailed description of the numerical procedure, however, is postponed to a separate publication. In addition, the authors annotate that if applied to a broader class of problems arising in the field of interacting boundary layers the technique presented here is even supposed to prove superior to miscellaneous well-established numerical schemes which are purpose-built for tackling such problems. Nevertheless, this is a topic which is yet under investigation.

2. Exemplary flow configurations

Numerical solutions have been obtained for several values of Λ whereas Γ varied in the whole range $0 \leq \Gamma \leq 1$. Owing to the limitation of space, only the case $\Lambda = 3$ will be discussed in detail. It then follows from Eq. (96) that $\chi = \Gamma^{10/3}/3$ and $0 \leq \chi \leq \chi_b$ with $\chi_b = 1/3$. Separation is associated with negative values of \hat{U}_s . As an important result, such local flow reversal is observed for $0 \leq \Gamma \leq \Gamma^*$ where $\Gamma^* \doteq 0.205$, that means within the (rather small) range $0 \leq \chi \leq \chi^*$ with $\chi^* \doteq 1.69 \times 10^{-3}$. We furthermore emphasize that the shear stress gradient at the surface, given by $\mathcal{Y} = (\partial \hat{T} / \partial \hat{Y})(\hat{X}, 0)$ as expressed in Eq. (126), and, in turn, both the Reynolds stress \hat{T} and the streamwise velocity gradient $\partial^2 \hat{\Psi} / \partial \hat{Y}^2$ are seen to be positive for all admissible values of \hat{X} , \hat{Y} , and χ .

Representative numerical results are plotted in figure 6 on the next page, where consecutive data points are connected using smooth cubic spline interpolation. In figures 6 (a) and (b) the positions at the surface $\hat{Y} = 0$ of flow detachment $\hat{X} = \hat{X}_D$ (dashed curves), flow reattachment $\hat{X} = \hat{X}_R$ (dotted curves), and their

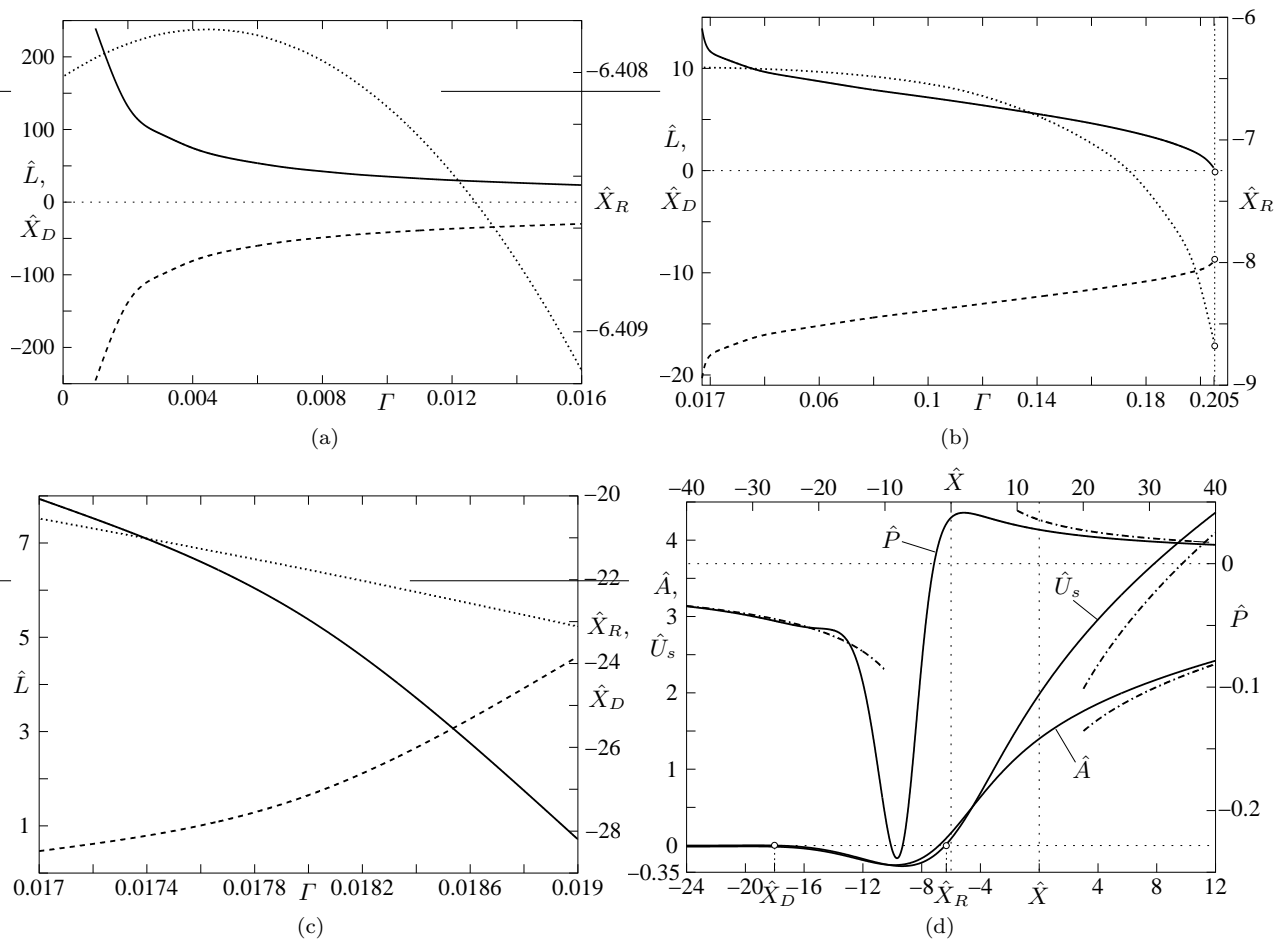


Figure 6. (a)–(c) Locations of detachment $\hat{X} = \hat{X}_D$, reattachment $\hat{X} = \hat{X}_R$, and bubble length $\hat{L} = \hat{X}_R - \hat{X}_D$ in dependence of Γ where (c) applies to the first-separating flow regime, (d) solutions for $\Gamma = 0.019$. Here $\hat{X}_D \doteq -18.01$ and $\hat{X}_R \doteq -6.40$. The abscissa at the bottom refers to \hat{A} and \hat{U}_s , the one at the top to \hat{P} .

difference, i.e. the length

$$\hat{L} = \hat{X}_R - \hat{X}_D \quad (128)$$

of the recirculation region (solid curves), are presented in the range $0 \leq \Gamma \leq 0.016$ and $0.017 \leq \Gamma \leq 0.205 \doteq \Gamma^*$, respectively. Note that the location of detachment tends to $-\infty$ for $\Gamma \rightarrow 0$, cf. Eq. (124). In turn, a rather flat separation bubble emerges for values of Γ within the range $0 < \Gamma < 0.017$. For larger values of Γ , i.e. for $\Gamma \geq 0.016 \dots$, up to $\Gamma = 0.019 \dots$ the interesting phenomenon of intermediate reattachment followed by a second flow detachment immediately further downstream is noticed. The corresponding values of \hat{X}_D , \hat{X}_R , and \hat{L} characterizing that first separated flow regime (which, however, appears to be very small and, therefore, difficult to resolve numerically) are shown in figure 6(c). Exemplarily, in figure 6(d) the distributions of $\hat{A}(\hat{X})$, $\hat{P}(\hat{X})$, and $\hat{U}_s(\hat{X})$ are displayed for the case $\Gamma = 0.019$, together with the upstream and downstream asymptotes (dashed-dotted lines) given by Eqs. (104), (103), (105), and (125). Note the rather flat passage of the quantities \hat{A} and \hat{U}_s to negative values compared to their pronounced rise downstream of reattachment. As a matter of fact, the indicated splitting of the separation bubble is hardly visible and, therefore, rather a conjecture at the present stage of the numerical analysis. Thus, its validation is effectively a topic of further numerical effort as it requires the use of an adequately refined mesh.

In addition, both the streamline pattern and the corresponding distributions of $\hat{\Psi}$ for various \hat{X} -locations for the reverse-flow regime of the identical flow configuration are depicted in figure 7. Note the increasing density of the streamlines further away from the surface and downstream of reattachment, the latter reflecting the strong acceleration there as represented by the correspondingly rapid rise of \hat{U}_s . The behavior of the streamlines in the vicinity of $\hat{X} = \hat{X}_D$ and \hat{X}_R , respectively, is discussed in §IV.C.3 below. The graphs shown in figure 7(b) agree well with the local analytical representation of $\hat{\Psi}$ given in Eq. (126).

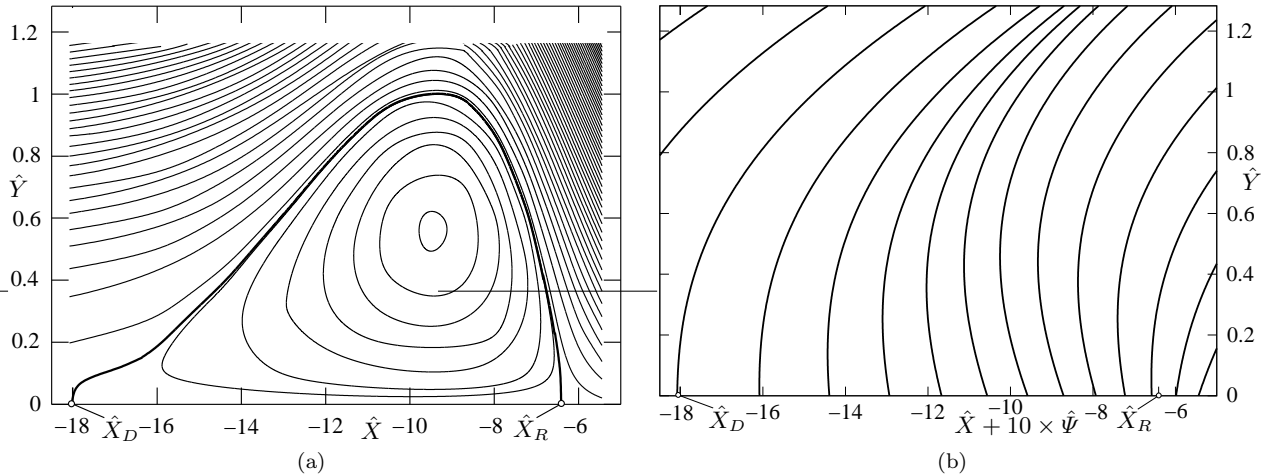


Figure 7. Separation for the case $\Gamma = 0.019$: (a) streamlines $\hat{\Psi} = \text{const}$ in the range $-0.085 \leq \hat{\Psi} \leq 1.01$ where Bezier spline interpolation was applied such that the values of $\hat{\Psi}$ for neighboring curves differ by 0.015, in addition, the dividing streamline (bold) is approximated by $\hat{\Psi} = 10^{-10}$ and is rather adjacent to the one where $\hat{\Psi} = -0.001$ which is also plotted, (b) several profiles of the stream function $\hat{\Psi}$ for the same \hat{X} - and \hat{Y} -range as in (a), magnified by a factor 10.

It is noteworthy that the rather rapid acceleration of the near-wall portion of the streamwise velocity immediately downstream of reattachment indicates an intense vortex motion there. This observation is in remarkable agreement with the findings of Perry and Fairlie,⁴² based on their heuristic inviscid flow model. However, here the step rise of \hat{U}_s owes to the specific internal structure of the flow ensuing from a non-trivial eigensolution of the triple-deck problem defined by Eqs. (115)–(119) and Eq. (112). This, in turn, owes to the strongly Reynolds-stress-affected downstream state of the solution enforced by the latter relationship.

3. Analysis of small backflow regions

Let $\hat{X} = \hat{X}_0$ denote the point of flow detachment or reattachment. Then the slip velocity and the induced pressure gradient behave as

$$\hat{U}_s = \hat{B}(\chi) \hat{S} + O(\hat{S}^2), \quad \hat{P}' = \hat{P}_0(\chi) + O(\hat{S}), \quad \hat{S} = \hat{X} - \hat{X}_0 \rightarrow 0, \quad (129)$$

where $\hat{B} < 0$, $\hat{S} < 0$ and $\hat{B} > 0$, $\hat{S} > 0$ in, respectively, the detaching and the reattaching case. Therefore, it is readily found from substituting the expression for \hat{U}_s in Eq. (129) into the first of the relationships (126), that the branching streamline having $\hat{\Psi} = 0$ is locally given by

$$\hat{Y}|_{\hat{\Psi}=0} \sim \frac{(15\hat{B})^{2/3}}{[16(1 + \Lambda\hat{P}_0)]^{1/3}} \hat{S}^{2/3}, \quad (130)$$

cf. figure 7 on the preceding page (a). The term in parentheses in the denominator of Eq. (130) represents the Reynolds stress gradient at the surface given by Υ , which is seen to be positive for all values of \hat{X} , cf. Eqs. (115) and (126), here evaluated for vanishing convection (that is, for $\hat{X} = \hat{X}_0$ it reduces to the overall pressure gradient $1 + \Lambda\hat{P}'$). In connection with the infinite streamline curvature at $\hat{S} = 0$ predicted by Eq. (130) it is interesting to note, that there is experimental evidence⁴³ that the streamline angle to the surface is not small even in the case of mild flow separation, despite the fact that the wall is flat. In this context the authors also refer to the statements given in Ref. 23 in respect of turbulent massive separation.

The points $\hat{X} = \hat{X}_D$ and $\hat{X} = \hat{X}_R$ denoting separation and reattachment, respectively, collapse onto the single point $\hat{X} = \hat{X}^*$ for $\chi = \chi^*$, so that $\hat{B}(\chi^*) = \hat{L} = 0$. Consequently, the emergence of a small closed reverse-flow regime is described by the relationships

$$\begin{aligned} \hat{U}_s &= \hat{B}_1(\hat{S}^2 - \hat{L}^2/4) + O(\hat{L}^3), & \hat{P}' &= \hat{P}_0(\chi^*) + O(\hat{L}), \\ \hat{X}_D &= \hat{X}^* - \hat{L}/2, & \hat{X}_R &= \hat{X}^* + \hat{L}/2, \\ \hat{S} &= \hat{X} - \hat{X}^* = O(\hat{L}), & \hat{L} &\rightarrow 0_+, \end{aligned} \quad (131)$$

where a match with the expression for U_s in Eq. (129) requires

$$\hat{B} = \mp \hat{B}_1 \hat{L} + O(\hat{L}^2), \quad \hat{B}_1 > 0. \quad (132)$$

Here the upper and the lower signs refer to, respectively, the position of separation and reattachment in Eq. (129). As the slip velocity \hat{U}_s varies with χ in a regular manner, the relations (131) state that \hat{L} depends on $\chi^* - \chi$ in the form

$$\hat{L} = O(\sqrt{\chi^* - \chi}), \quad \chi^* - \chi \rightarrow 0_+. \quad (133)$$

This property is captured by the behavior of the numerical results near the endpoints of the curves, indicated by circles, where $\Gamma = \Gamma^*$ in figure 6 (b). In addition, one readily finds that the streamlines $\hat{\Psi} = \text{const}$ in the vicinity of a very mild separation bubble of length $\hat{L} \ll 1$ are given by

$$\hat{B}_1 \left(\hat{S}^2 - \frac{\hat{L}^2}{4} \right) \hat{Y} + \frac{4}{15} \sqrt{1 + \Lambda\hat{P}_0(\chi^*)} \hat{Y}^{5/2} \sim \hat{\Psi}, \quad \hat{S} = O(\hat{L}), \quad \hat{Y} = O(\hat{L}^{4/3}). \quad (134)$$

Finally, it should be mentioned that, from a computational point of view, the triple-deck formulation presented here is related to the original numerical treatment of transient marginal separation past the leading edge of an airfoil by Briley and McDonald.⁴⁴ They employed an advanced mixing-length-based one-equation closure and adopted a time-dependent iterative scheme which reflects the interaction process, albeit in a non-asymptotic sense. This technique allowed for avoiding the occurrence of the Goldstein singularity in the skin friction in the boundary layer sweeps and the prediction of closed separation bubbles.

V. Conclusions and Further Outlook

An asymptotic theory of turbulent marginal separation has been presented which depends on a single similarity parameter $\chi \geq 0$ containing the essential upstream information. Numerical solutions of the fundamental triple-deck problem have been found for a wide range of χ . Open questions include, among others,

the effect of the exponentially decaying eigensolutions as $\hat{X} \rightarrow -\infty$ which dominate over the algebraically varying terms for $\Gamma = 1$ in the non-interactive case $\Lambda \rightarrow 0$ or, equivalently, $\chi \rightarrow \infty$ as predicted by Eq. (124). Then only the strictly attached solutions have been found at present, which are related to the sub-critical upstream condition $\gamma < 0$. Its super-critical counterpart $\gamma > 0$, however, causing the boundary layer solution to terminate in the Goldstein-type singularity, is likely associated with a very large recirculation region if the induced pressure is taken into account in an appropriate manner. That is, the triple-deck problem has to be investigated in order to explore the according sub-structure emerging for $\Lambda \rightarrow 0$ and predicting separation on a correspondingly larger streamwise length scale. Interestingly, the assumption of an almost inviscid but strongly rotational flow inside the separation region proposed much earlier by Perry and Fairlie⁴² is possibly pointed to the inviscid character of the boundary layer solution slightly upstream of the position of breakdown, see §III.D. This observation may therefore become relevant to the study of large-scale separation.

Furthermore, the effects of the inner wake as well as the Reynolds-number-dependent flow regimes adjacent to the surface have to be studied. However, the inner wake layer, not considered here, is seen to behave only passively as it is characterized by convective terms linearized about the slip velocity imposed by the outer wake. Since $\alpha \ll 1$ even in the limiting case $Re^{-1} = 0$, the perturbations in the wake regime reflecting viscous effects, which primarily arise from the surface shear stress denoted by τ , are of minor (physical) relevance. On the other hand, most important, matching of the logarithmically varying u -components of the velocities in the overlap domain of the viscosity-affected near-wall flow regimes gives rise to a relationship determining the surface friction τ in the limit $Re \rightarrow \infty$,

$$\frac{\sqrt{\tau}}{u_s} \sim \frac{\kappa}{\ln Re}, \quad \tau = \frac{1}{Re} \frac{\partial u}{\partial y} \quad \text{at } y = 0. \quad (135)$$

That skin friction law is clearly rendered invalid if the surface slip velocity u_s at the base of the wake tends to zero which is the case as separation is approached. Therefore, the investigation of a flow on the verge of separation where the reverse-flow regime is governed by Eq. (134) is expected to give a first hint how to continue the skin friction law (135) asymptotically correctly into the regions where the flow separates but immediately recovers. It can be shown^{11,12} that both $\sqrt{\tau}$ and u_s become quantities of $O(1)$ provided that u_s has dropped sufficiently. Then the logarithmic law of the wall is superseded by the half-power behavior of u , well-known from a boundary layer on the verge of separation, as the viscous wall layer coincides with the flow regime on top of it, see the outline in §II.B.2, and the relationship (135) ceases to be valid. Since the flow inside the viscous wall layer then plays a fundamental role in order to predict the surface friction, a study of the time-dependent motions in that region is presumably necessary. The basis for such a research is provided by the extensive work of Walker,¹⁴ Walker and Herzog,¹⁵ and Brinckman and Walker,¹⁶ see also Ref. 1, which, however, applies to a firmly attached turbulent boundary layer.

With respect to those aspects, which are presently under investigation, we add that results obtained by means of Direct Numerical Simulation (DNS)⁴⁵ indicate that small changes in the pressure distribution due to an external flow which triggers the occurrence of a mild separation bubble have a relatively great impact on the skin friction distribution. Here we stress that this observation is corroborated by the theory presented as the slip velocity is related to the skin friction through Eq. (135). A qualitative comparison of the theory outlined here with the DNS study of marginal separation by Na and Moin⁴⁶ as well as the Large-Eddy Simulation by Cabot⁴⁷ for the identical flow configuration is a topic of current research also. Unfortunately, a validation of the theoretical results with experimental data, although highly desirable, appears to be impossible on the basis of the existing material.

Acknowledgments

This work was supported by the Austrian Science Fund (FWF) under Grant No. P16555-N12. Also, the authors would like to thank the referees for several helpful suggestions and advices which aided to enhance the quality of the paper.

References

¹Walker, J. D. A., “Turbulent Boundary Layers II: Further Developments,” *Recent Advances in Boundary Layer Theory*, edited by A. Kluwick, Vol. 390 of *CISM Courses and Lectures*, Springer, Vienna, New York, 1998, pp. 145–230.

- ²Degani, A. T., Smith, F. T., and Walker, J. D. A., “The Structure of a Three-Dimensional Turbulent Boundary Layer,” *Journal of Fluid Mechanics*, Vol. 250, 1993, pp. 43–68.
- ³Degani, A. T., Smith, F. T., and Walker, J. D. A., “The Three-Dimensional Turbulent Boundary Layer near a Plane of Symmetry,” *Journal of Fluid Mechanics*, Vol. 234, 1992, pp. 329–360.
- ⁴Yajnik, K. S., “Asymptotic Theory of Turbulent Shear Flows,” *Journal of Fluid Mechanics*, Vol. 42, No. 2, 1970, pp. 411–427.
- ⁵Bush, W. B. and Fendell, F. E., “Asymptotic Analysis of Turbulent Channel and Boundary-Layer Flow,” *Journal of Fluid Mechanics*, Vol. 56, No. 4, 1972, pp. 657–681.
- ⁶Fendell, F. E., “Singular Perturbation and Turbulent Shear Flow near Walls,” *The Journal of the Astronautical Sciences*, Vol. 20, No. 11, 1972, pp. 129–165.
- ⁷Mellor, G. L., “The Large Reynolds Number, Asymptotic Theory of Turbulent Boundary Layers,” *International Journal of Engineering Science*, Vol. 10, No. 10, 1972, pp. 851–873.
- ⁸Schlichting, H. and Gersten, K., *Boundary-Layer Theory*, Springer, Berlin, Heidelberg, Germany, 8th ed., 2000.
- ⁹Gersten, K., “Turbulent Boundary Layers I: Fundamentals,” *Recent Advances in Boundary Layer Theory*, edited by A. Kluwick, Vol. 390 of *CISM Courses and Lectures*, Springer, Vienna, New York, 1998, pp. 107–144.
- ¹⁰Scheichl, B. F., *Asymptotic Theory of Marginal Turbulent Separation*, Ph.D. thesis, Vienna University of Technology, Vienna, Austria, June 2001.
- ¹¹Scheichl, B. and Kluwick, A., “On Turbulent Marginal Separation: How the Logarithmic Law of the Wall is Superseded by the Half-Power Law,” *BAIL 2006. International Conference on Boundary and Interior Layers. Göttingen, 24th – 28th July, 2006. Proceedings*, edited by G. Lube and G. Rapin, Georg-August University Göttingen, Göttingen, Germany, 2006, Contributed Presentations, on CD-ROM, see also <http://www.num.math.uni-goettingen.de/bail/>.
- ¹²Scheichl, B. and Kluwick, A., “Turbulent Marginal Separation: A Novel Triple-Deck Problem for Turbulent Flows,” *Progress in Turbulence II*, edited by J. Peinke, A. Kittel, S. Barth, and M. Oberlack, Springer Proceedings in Physics, Springer, Berlin, Heidelberg, New York, 2006, to be published.
- ¹³Nagib, H. M. and Chauhan, K. A., “Scaling of High Reynolds Number Turbulent Boundary Layers Revisited,” AIAA Paper 2005-4810, American Institute of Aeronautics and Astronautics (AIAA), 2005.
- ¹⁴Walker, J. D. A., Abbott, D. E., Scharnhorst, R. K., and Weigand, G. G., “Wall-Layer Model for the Velocity Profile in Turbulent Flows,” *AIAA Journal*, Vol. 27, No. 2, 1989, pp. 140–149.
- ¹⁵Walker, J. D. A. and Herzog, S., “Eruption Mechanisms for Turbulent Flows near Walls,” *Transport Phenomena in Turbulent Flows: Theory, Experiment, and Numerical Simulation. Proceedings of the 2nd International Symposium on Transport Phenomena in Turbulent Flows, Tokyo, October 1987*, edited by M. Hirata and N. Kasagi, Hemisphere, New York, Washington, Philadelphia, London, 1988, pp. 145–156.
- ¹⁶Brinckman, K. W. and Walker, J. D. A., “Instability in a Viscous Flow Driven by Streamwise Vortices,” *Journal of Fluid Mechanics*, Vol. 432, 2001, pp. 127–166.
- ¹⁷Smith, C. R. and Walker, J. D. A., “Chapter VI. Turbulent Wall-Layer Vortices,” *Fluid Vortices*, edited by S. I. Green, Vol. 30 of *Fluid Mechanics and its Applications*, Kluwer Academic, Dordrecht, Boston, London, 1995, pp. 135–290.
- ¹⁸Ruban, A. I., “Singular Solutions of the Boundary Layer Equations Which Can Be Extended Continuously Through the Point of Zero Surface Friction,” *Fluid Dynamics*, Vol. 16, No. 6, 1981, pp. 835–843, original Russian article in *Izvestiya Akademii Nauk SSSR, Mekhanika Zhidkosti i Gaza*, No. 6, 1981, pp. 42–52.
- ¹⁹Ruban, A. I., “Asymptotic Theory of Short Separation Regions on the Leading Edge of a Slender Airfoil,” *Fluid Dynamics*, Vol. 17, No. 1, 1982, pp. 33–41, original Russian article in *Izvestiya Akademii Nauk SSSR, Mekhanika Zhidkosti i Gaza*, No. 1, 1982, pp. 42–51.
- ²⁰Stewartson, K., Smith, F. T., and Kaups, K., “Marginal Separation,” *Studies in Applied Mathematics*, Vol. 67, No. 1, 1982, pp. 45–61.
- ²¹Sychev, V. V., Ruban, A. I., Sychev, Vic. V., and Korolev, G. L., *Asymptotic Theory of Separated Flows*, Cambridge University Press, Cambridge, UK, 1998.
- ²²Scheichl, B. and Kluwick, A., “Singular Solutions of the Turbulent Boundary Layer Equations in the Case of Marginal Separation as $Re \rightarrow \infty$,” *Advances in Turbulence IX. Proceedings of the Ninth European Turbulence Conference held in Southampton, U.K., July 2–5, 2002*, edited by I. P. Castro, P. E. Hancock, and T. G. Thomas, International Center for Numerical Methods in Engineering (CIMNE), Barcelona, 2002, pp. 829–832.
- ²³Neish, A. and Smith, F. T., “On Turbulent Separation in the Flow past a Bluff Body,” *Journal of Fluid Mechanics*, Vol. 241, 1992, pp. 443–467.
- ²⁴Melnik, R. E., “A New Asymptotic Theory of Turbulent Boundary Layers and the Turbulent Goldstein Problem,” *Boundary-Layer Separation. Proceedings of the IUTAM Symposium, London, August 26–28, 1986*, edited by F. T. Smith and S. N. Brown, Springer, New York, Heidelberg, Berlin, 1987, pp. 217–234.
- ²⁵Melnik, R. E., “An Asymptotic Theory of Turbulent Separation,” *Computers & Fluids*, Vol. 17, No. 1, 1989, pp. 165–184.
- ²⁶Michel, R., Quémar, C., and Durant, R., “Hypothesis on the Mixing Length and Application to the Calculation of the Turbulent Boundary Layers,” *Proceedings of Computations of Turbulent Boundary Layers – 1968 AFOSR-IFP-Stanford Conference*, edited by S. J. Kline, M. V. Morkovin, G. Sovran, and D. J. Cockrell, Vol. 1, Stanford University, Stanford, CA, 1969, pp. 195–207.
- ²⁷Clauser, F. H., “The Turbulent Boundary Layer,” *Advances in Applied Mechanics*, edited by H. Dryden and Th. v. Kármán, Vol. 4, Academic, New York, 1956, pp. 1–51.
- ²⁸Goldstein, S., “On Laminar Boundary Layer Flow near a Position of Separation,” *The Quarterly Journal of Mechanics and Applied Mathematics*, Vol. 1, No. 1, 1948, pp. 43–69.
- ²⁹Stewartson, K., “Is the Singularity at Separation Removable?” *Journal of Fluid Mechanics*, Vol. 44, No. 2, 1970, pp. 347–364.

- ³⁰Schneider, W., "Boundary-Layer Theory of Free Turbulent Shear Flows," *Zeitschrift für Flugwissenschaften und Weltraumforschung (Journal of Flight Sciences and Space Research)*, Vol. 15, No. 3, 1991, pp. 143–158.
- ³¹Klebanoff, P. B., "Characteristics of Turbulence in a Boundary Layer with Zero Pressure Gradient," NACA Technical Report 1247, NASA Langley Research Center, Hampton, VA, 1955, also NACA Technical Note 3178, 1954.
- ³²Skåre, P. E. and Krogstad, P.-Å., "A Turbulent Equilibrium Boundary Layer near Separation," *Journal of Fluid Mechanics*, Vol. 272, 1994, pp. 319–348.
- ³³Rothmayer, A. P. and Smith, F. T., "Part III: High Reynolds Number Asymptotic Theories," *The Handbook of Fluid Dynamics*, edited by R. W. Johnson, CRC Press, Boca Raton, FL (also Springer, Heidelberg, Germany), 1998, pp. III.1–25.26.
- ³⁴Messiter, A. F., "Boundary-Layer Flow near the Trailing Edge of a Flat Plate," *SIAM Journal on Applied Mathematics*, Vol. 18, No. 1, 1970, pp. 241–257.
- ³⁵Stewartson, K., "On the Flow near the Trailing Edge of a Flat Plate II," *Mathematika*, Vol. 16, No. 1, 1969, pp. 106–121.
- ³⁶Abramowitz, M. and Stegun, I. A., *Handbook of Mathematical Functions*, Dover, New York, 9th ed., 1972.
- ³⁷Lipatov, I. I., "On the Theory of Separation of a Laminar Boundary Layer in a Supersonic Flow," *Fluid Dynamics*, Vol. 19, No. 4, 1984, pp. 555–560, original Russian article in *Izvestiya Akademii Nauk SSSR, Mekhanika Zhidkosti i Gaza*, No. 4, 1984, pp. 51–56.
- ³⁸Smith, F. T. and Merkin, J. H., "Triple-Deck Solutions for Subsonic Flows past Humps, Steps, Concave or Convex Corners and Wedged Trailing Edges," *Computers & Fluids*, Vol. 10, No. 1, 1982, pp. 7–25.
- ³⁹Cassel, K. W., Ruban, A. I., and Walker, J. D. A., "An Instability in Supersonic Boundary-Layer Flow over a Compression Ramp," *Journal of Fluid Mechanics*, Vol. 300, 1995, pp. 265–285.
- ⁴⁰Gajjar, J. S. B. and Türkyılmazoğlu, M., "On the Absolute Instability of the Triple-Deck Flow over Humps and near Wedged Trailing Edges," *Philosophical Transactions of the Royal Society, Series A: Mathematical, Physical and Engineering Sciences*, Vol. 358, No. 1777, 2000, pp. 3113–3128.
- ⁴¹Powell, M. J. D., "A Hybrid Method for Nonlinear Algebraic Equations," *Numerical Methods for Nonlinear Algebraic Equations*, edited by P. Rabinowitz, Gordon and Breach, London, 1970, pp. 87–114, Chapter 6.
- ⁴²Perry, A. E. and Fairlie, B. D., "A Study of Turbulent Boundary-Layer Separation," *Journal of Fluid Mechanics*, Vol. 69, No. 4, 1975, pp. 657–672.
- ⁴³Cutler, A. D. and Johnston, J. P., "Adverse Pressure Gradient and Separating Turbulent Boundary Flows: The Effect of Disequilibrium in Initial Conditions," Stanford Report MD-46, Thermosciences Division, Mechanical Engineering Department, Stanford University, Stanford, CA, 1984.
- ⁴⁴Briley, W. R. and McDonald, H., "Numerical Prediction of Incompressible Separation Bubbles," *Journal of Fluid Mechanics*, Vol. 69, No. 4, 1975, pp. 631–656.
- ⁴⁵Skote, M. and Henningson, D. S., "Direct Numerical Simulation of a Separated Turbulent Boundary Layer," *Journal of Fluid Mechanics*, Vol. 471, 2002, pp. 107–136.
- ⁴⁶Na, Y. and Moin, P., "Direct Numerical Simulation of a Separated Turbulent Boundary Layer," *Journal of Fluid Mechanics*, Vol. 374, 1998, pp. 379–405.
- ⁴⁷Cabot, W., "Large-Eddy Simulation of a Separated Boundary Layer," *Annual Research Briefs 1998*, Center for Turbulence Research, NASA/Ames, Stanford University, Stanford, CA, 1998, pp. 279–287.